JOURNAL OF PETROLOGY | VOLUME 37 | NUMBER 3 | PAGES 497–519 | 1996

STEFAN BERNSTEIN[1]*, PETER B. KELEMEN[2] AND C. KENT BROOKS[1,3]
[1]DANISH LITHOSPHERE CENTRE, ØSTER VOLDGADE 10, DK-1350 COPENHAGEN K, DENMARK
[2]WOODS HOLE OCEANOGRAPHIC INSTITUTION, WOODS HOLE, MA 02543, USA
[3]GEOLOGICAL INSTITUTE, UNIVERSITY OF COPENHAGEN, ØSTER VOLDGADE 10, DK-1350 COPENHAGEN K, DENMARK

Evolution of the Kap Edvard Holm Complex: a Mafic Intrusion at a Rifted Continental Margin

The Kap Edvard Holm Layered Series forms part of the East Greenland Tertiary Province, and was emplaced at shallow crustal level (at depths corresponding to a pressure of 1–2 kbar) during continental break-up. It consists of two suites: a gabbro suite comprising olivine and oxide gabbros, leucocratic olivine gabbros and anorthosites, and a suite of wehrlites that formed from the intrusion of the gabbros during their solidification by a hydrous, high-MgO magma. Ion microprobe analyses of clinopyroxene reveal chemical contrasts between the parental melt of the wehrlite suite and that of the gabbro suite. Thin sills (1–2 m thick) of the wehrlite suite, however, have clinopyroxene compositions similar to the gabbro suite, and were formed by interaction with interstitial melts from the host layered gabbros. All evolved members of the gabbro suite have elevated Nd, Zr and Sr concentrations and Nd/Yb ratios, relative to the melt parental to the gabbro suite. These characteristics are attributed to establishment of a magma chamber at depths corresponding to a pressure of 10 kbar, where melts evolved before injection into the low-pressure magma chamber. Anorthosites of the gabbro suite are believed to have crystallized from such injections. The melts became supersaturated in plagioclase by the pressure release that followed transportation to the low-pressure magma chamber after initial fractionation at ~10 kbar. The most evolved gabbros formed by subsequent fractionation within the low-pressure magma chamber. Our results indicate that high-pressure fractionation may be important in generating some of the lithological variations in layered intrusions.

KEY WORDS: *fractionation; ion microprobe; layered intrusions; rift processes; trace elements*

INTRODUCTION

The classical approach to estimating the composition of the melts parental to mafic intrusions has been the sampling of chilled margins from the contact zones (Wager, 1960; Hoover, 1978). As discussed by Ford (1981) and Hoover (1989), this method, although it may be pertinent to the investigation of intrusions that crystallized from a single batch of magma (such as the Skaergaard intrusion), is not appropriate for intrusive complexes that appear to have crystallized from multiple replenishment episodes. In this case, the chilled margin method provides no constraints on how representative the chosen sample is of the bulk of the intrusive complex. Another problem is encountered when characterizing the nature of the crystallization processes that were active during the formation of mafic intrusions. Crystallization processes are typically addressed by studying the major-element variations in cumulus phases. Although major-element variations of cumulus phases provide a qualitative measure of the degree of fractionation and of replenishment events, calculation of melt compositions from major-element mineral data is severely hampered by the continuous re-equilibration of major elements in ferro-magnesian minerals during post-cumulus melt migration, and the subsequent subsolidus equilibration of intra-crystalline chemical gradients (e.g. Scowen *et al.*, 1991). In contrast, silicate phases potentially retain their concentration gradients in high valence trace-elements, owing to their considerably lower diffusivities in minerals compared with diffusivities of most major elements (Freer, 1981; Watson & Baker, 1992). Furthermore, partition coefficients for several

---

*Corresponding author.

trace-elements deviate substantially from unity and their incorporation in cumulus phases therefore records the characteristics of the crystallization processes. The ion microprobe is ideal for determining the trace-element concentrations in silicates. On the basis of these concentrations, equilibrium melt concentrations may be calculated, using published partition coefficients. Clinopyroxene is present in all mafic and ultramafic lithologies from the Kap Edvard Holm Layered Series, and the partition coefficients between clinopyroxene and basaltic melts are fairly well constrained. This phase therefore forms the basis for a trace-element study of the crystallization history of this intrusive complex.

GEOLOGICAL SETTING

The Kap Edvard Holm Layered Series (KEHLS) was emplaced into the volcanic margin of the central Greenland Archaean craton during the opening of the North Atlantic Ocean (Fig. 1) (Wager, 1934; Abbott & Deer, 1972; Myers, 1980; Brooks & Nielsen, 1982*a*, 1982*b*). The earliest recorded volcanic event in the East Greenland Tertiary Province was the outpouring of a series of heterogeneous basalts, including picrites, now mainly exposed around the mouth of the Kangerlussuaq Fjord (Soper *et al.*, 1976; Nielsen *et al.*, 1981). The majority of the overlying plateau basalts are chronologically confined to magnetic anomaly 24R, i.e. 57–55 m.y., with intermittent activity well into the mid-Eocene (Brooks *et al.*, 1976; Soper *et al.*, 1976; Larsen & Watt, 1985; Larsen *et al.*, 1989). In addition to flood basalts and dyke swarms, several tholeiitic intrusives like the KEHLS are exposed along the coast (Wager, 1934; Brooks & Nielsen, 1982*a*). The layered mafic intrusions have generally been intruded immediately before the flexure that affected the coastal area at the latest stages of flood basalt formation (Wager, 1934; Myers, 1980; Brooks & Nielsen, 1982*b*; Bott, 1987). Some of the large tholeiitic intrusions (including the Skaergaard intrusion and the KEHLS) appear to be emplaced at the contact between the Archaean basement and the overlying basalt–sediment pile (Wager, 1947; Irvine, 1987; Bird *et al.*, 1988; Myers *et al.*, 1993).

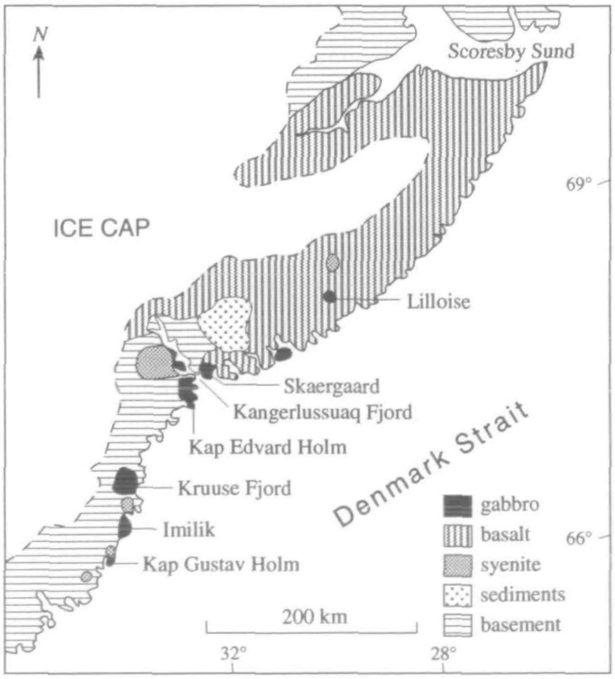

Fig. 1. Regional map of the East Greenland Tertiary Province. The erosional level south of the Kangerlussuaq Fjord is deeper, exposing plutons that have been covered with flood basalts.

Previous studies on the KEHLS (Abbott & Deer, 1972; Bernstein *et al.*, 1992; Tegner *et al.*, 1993) have concluded that the complex crystallized from a dry tholeiitic magma, and that the restricted range in modal composition of the gabbros and in the compositional variation of the cumulus minerals was due to frequent replenishments of less differentiated melts. In this respect, the KEHLS shares chemical and structural features with layer three in the oceanic crust, as revealed by the large gabbroic sequences in ophiolites (e.g. Pallister & Hopson, 1981; Brooks & Nielsen, 1982*b*). On these grounds and on the basis of field evidence, Bernstein *et al.* (1992) suggested that the KEHLS served as a shallow-level reservoir for basaltic flows during the waning stages of the flood basalt magmatism.

Bernstein *et al.* (1992) also documented the existence of two distinct magmatic suites in the KEHLS. The most voluminous is termed the 'gabbro suite' and constitutes the layered gabbros, which mostly are plagioclase–clinopyroxene–olivine or plagioclase–clinopyroxene–(Fe–Ti)-oxide cumulates (see below). The second magmatic suite occurs as ultramafic or melanocratic sills and small plugs within the layered gabbros, and is termed the 'wehrlite suite' (Bernstein *et al.*, 1992; Tegner & Wilson, 1993), and is a further similarity to classic ophiolite occurrences (e.g. Benn & Laurent, 1987; Juteau *et al.*, 1988).

PETROLOGY OF KEHLS

Descriptions of the KEHLS have been given by Deer & Abbott (1965), Wager & Brown (1968), Elsdon (1969, 1971), Abbott & Deer (1972), Bernstein *et al.* (1992), Tegner *et al.* (1993) and Tegner & Wilson, (1993). Below is a brief account of the gabbro suite that makes up the bulk of the intrusion, and of the volumetrically subordinate wehrlite suite.

The gabbro suite

The bulk KEHLS comprises olivine (ol) gabbros and Fe–Ti oxide (ox) gabbros, with modal cumulus assemblages of plagioclase–clinopyroxene–olivine (plag–cpx–ol) and plag–cpx–(Fe–Ti) oxide (± ol), in order of decreasing modal abundance. On the basis of cumulus assemblages and major changes in composition of cumulus minerals, the KEHLS has been divided into a Lower Layered Series (LLS), a Middle Layered Series (MLS) and an Upper Layered Series (ULS) (Deer & Abbott, 1965; Elsdon, 1969; Abbott & Deer, 1972; Bernstein *et al.* 1992) (Figs 1 and 2). The ULS may represent the roof-zone of the magma chamber, and comprises layered oxide gabbros and anorthosite lenses. The ULS lithologies are heavily affected by hydrothermal alteration, possibly caused by the emplacement of nearby syenite bodies to the south. The LLS is dominated by ol gabbros that in places are succeeded by ox gabbros (Bernstein *et al.*, 1992). A 2000 m stratigraphic package reveals several reversals to more primitive mineral compositions and modal assemblages, suggesting repeated influxes of fresh, less differentiated magma (Bernstein *et al.*, 1992; Bird *et al.*, 1995). The MLS is made up by a number of thick, cyclic units (average thickness of 80 m; Tegner *et al.*, 1993) that appear to cut the LLS, although the contact to the LLS is not exposed (Fehlhaber & Bird, 1991). The base of the MLS is composed of anorthosites grading into poikilitic ol gabbros, suggesting the crystallization sequence: plagioclase–olivine/clinopyroxene. In general for all three series, it appears that when reversals to less differentiated compositions are found in the cumulus minerals, suggesting new pulses of magma, the gabbros are more leucocratic relative to the more evolved samples, reflecting higher modal proportions of plagioclase. This is especially evident in the basal anorthositic part of the MLS. Only in one instance has a new pulse of magma given rise to a rather thin (3–4 m thick), sill-like, melanocratic gabbroic unit (sample 61, see below) which grades into a 'normal' ol gabbro within 5–10 m. The above-described rocks are believed to be cogenetic, because there is a gradual transition from all primitive 'end-members' (anorthosites and ultramafic layers) to the ol gabbros and ox gabbros. In addition, all rocks of the gabbro suite have very low contents of primary magmatic hydrous minerals, contrasting with the wehrlite suite described below.

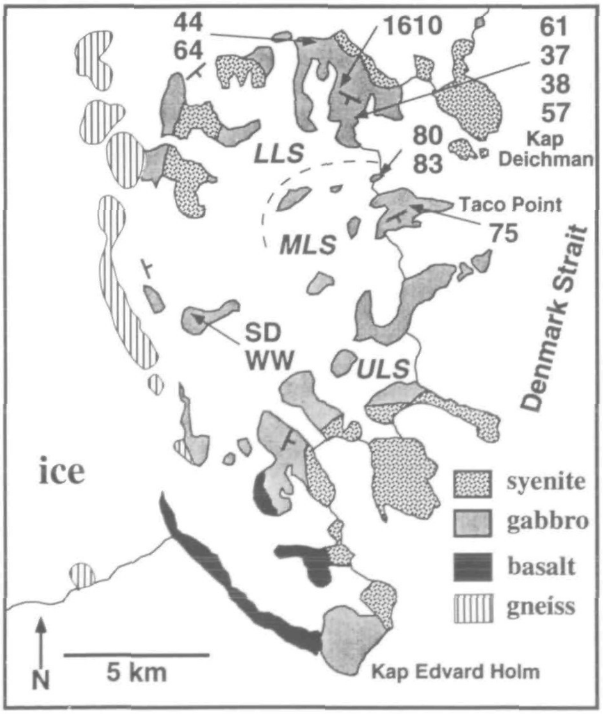

Fig. 2. Map of the Kap Edvard Holm Layered Series, showing the location of samples referred to in the text. LLS, MLS and ULS—Lower, Middle and Upper Layered Series, respectively. Average orientation of layering is indicated. The wehrlite suite is not voluminous enough to make mappable units.

The wehrlite suite

The wehrlite suite (<1% of the total volume of intrusive rocks) is typically manifested as sills of 50 cm to 1 m thickness in the layered gabbros, although a considerable span in thicknesses is observed. The thinnest (about 2–3 cm thick) are hardly distinguishable from melanocratic layers in the layered gabbroic sequence, whereas the thickest are >10 m thick and can be traced to the limit of outcrop (up to 3 km). Discordant pipes of wehrlite in the layered gabbros and slump-like structures at the contact between wehrlite sill and host layered gabbro are commonly observed. Replacement structures resulting from interaction between the intrusive ultramafic melt and the host gabbro also occur, especially in the MLS (Tegner & Wilson, 1993). Wehrlite sills occur throughout the entire intrusion with an average abundance of one sill per 50 m of stratigraphic section. A large, irregular body (minimum 30 m × 40 m × 100 m) of wehrlite (hereafter the wehrlite plug) is emplaced into the LLS (sample 1610 in Fig. 2).

As described by Bernstein *et al.* (1992) and Tegner & Wilson (1993), field evidence suggests that the primitive magma, which formed the sills of the wehrlite suite, intruded at a stage where the host layered gabbros were not completely solidified. The rocks of the wehrlite suite have magmatic amphibole and phlogopite crystals, whereas the host layered gabbros are virtually devoid of magmatic hydrated phases. Phlogopite crystals show evidence of deformation, suggesting that the mica crystallized before emplacement. The rocks of the wehrlite suite are also generally coarser grained and have higher modal contents of olivine (30–70%) compared with the host gabbros (0–20%).

PETROGRAPHY

A total of 12 samples were selected for trace-element analysis. Six samples are from the KEHLS gabbros, six are from the wehrlite suite including five sills and the wehrlite plug sample 1610 (see Table 1 and Figs 1 and 2). The following is a brief description of the individual samples, starting with the gabbro suite (see Fig. 2 for sample locations). Representative major element analyses for minerals from some of the samples have been given by Bernstein *et al.* (1992) and Tegner & Wilson (1993) (sample number in parentheses).

Sample 61 (61xx), gabbro suite, is the most primitive representative of this suite. It is a melanocratic olivine gabbro, with a sharp lower contact to some 'normally' layered, mesocratic olivine gabbros of the LLS. The upper contact is less distinct, and there is evidence of disturbance in the surrounding gabbros, with slumping and recumbent folds. The contact relations suggest that the melanocratic gabbro formed by injection of primitive magma into a layered gabbro mush, thus resembling the sills of the wehrlite suite. The estimated thickness of this unit is ~3 m, and the sample comes from ~0·5 m above the lower contact. Olivine and some clinopyroxenes are coarse (up to 5 mm), whereas plagioclase and part of the clinopyroxenes form a fine-grained intergrowth, where clinopyroxene typically displays poikilitic texture. Olivine, which is somewhat altered, has inclusions of anhedral chromium spinel. The large clinopyroxenes are strongly zoned (optically and chemically), some are euhedral to subhedral, and some have skeletal morphology, with evidence of resorbed cores (Fig. 3). The fine-grained poikilitic clinopyroxenes usually appear as an overgrowth on the euhedral and skeletal clinopyroxene crystals, so that the original euhedral shape is preserved in the zoning pattern. There is a fine-grained matrix consisting of talc and actinolite, some of which could result from hydrothermal alteration of fine-grained olivine. Therefore the proportions of phases in the sample are difficult to estimate, but roughly it consists of 30% olivine, 30% clinopyroxene, 20% plagioclase and 20% altered material. As the plagioclase crystals are fresh, the altered material probably originated as mafic phases, i.e. olivine or possibly orthopyroxene. With *mg*-number [molar Mg/(Mg + Fe)] of up to 90 for the clinopyroxene cores, this sample represents the most primitive melt yet found in the KEHLS.

Sample 64, gabbro suite, comes from some of the lowermost exposures of the LLS. The sample is representative of a package of fairly uniform, well-layered olivine gabbros, some 300–500 m in thickness, that is interrupted only by a few melanocratic sills of 0·5–1 m thickness belonging to the wehrlite suite (see sample 44). The texture is granular, and fine to medium grained, except for the occasional occurrence of elongated olivine crystals. The sample contains ~50–60% plagioclase, 25–30% clinopyroxene and 15–20% olivine. With *mg*-number ~79 for clinopyroxenes, the sample is typical for the primitive end of 'normal' gabbros from the KEHLS.

Table 1: Sample collection of the present study

Sample no.	Sample no.*	Location	Rock type	cpx *mg*-no.	No. analyses†
Gabbro suite					
312361	61	LLS	ol gabbro ml	75–90	12
352184	64	LLS	ol gabbro ms	79–80	6
312380	80	MLS	ol gabbro lc	76–78	4
312383	83	MLS	anorthosite–lc gabbro	78–80	6
312337	37	LLS	ox gabbro ms	73–76	2
312338	38	LLS	ox gabbro ms	73–76	7
Wehrlite suite					
1610	1610	LLS	wehrlite	85–88	12
PCT 75	75	MLS	wehrlite	79–81	5
WW	WW	ULS	wehrlite	76–77	3
SD	SD	ULS	ol gabbro ml	73–76	3
312357	57	LLS	ol gabbro ml	74–77	7
352144	44	LLS	ol gabbro ml	78–81	10

LLS, MLS and ULS—Lower, Middle and Upper Layered Series, respectively. ml, ms and lc—melanocratic, mesocratic and leucocratic, respectively.

*Abbreviated, as presented in figures.

†Total number of ion microprobe spot analyses of cpx in each sample.

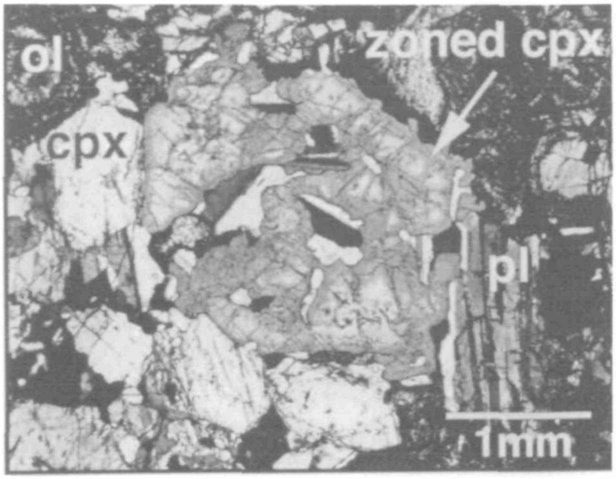

Fig. 3. Clinopyroxene crystal in the melanocratic sill sample 61. The crystal is strongly zoned—lighter areas are Al, Mg and Cr rich. The darker areas, which are the rims and poikilitic overgrowth (upper left corner), are compositionally identical to clinopyroxene from the layered gabbro series (see Fig. 5).

Samples 37 and 38, gabbro suite, are medium-grained, well-laminated orthocumulates. They are oxide gabbros, with very little olivine (0–5%, always extensively altered), and their general modal compositions are 55% plagioclase, 30–35% clinopyroxene and 5–10% Fe–Ti oxides, with average grain-size of ~2 mm. They represent the most evolved gabbros in the sample collection, as reflected in their relatively low *mg*-number (~75; Table 1). The oxide gabbros come from a section of well-laminated and layered gabbros, which give an impression of a quiet state in the crystallization of the KEHLS magma chamber in the stratigraphic interval 900–1300 m [as described by Bernstein *et al.* (1992); the samples are from the 1200 m level], with unusual continuous layering and absence of both deformation features and intrusive wehrlite sills. The two samples are spaced ~10 m apart.

Sample 80, gabbro suite, is a leucocratic olivine gabbro. This, and sample 83 (see below), represent the lowermost exposure of the MLS, which is very heterogeneous, with discontinuous bands and layers, slump-structures and other signs of an unstable magma chamber. Sample 80 is granular and medium grained, with few signs of hydrothermal alteration. The modal composition is 60–65% plagioclase, 15–20% clinopyroxene and 10–15% olivine, plus minor amount of Fe–Ti oxides. Clinopyroxene crystals are 2–3 mm in size and slightly poikilitic, enclosing small (0·1–0·5 mm) plagioclase crystals.

Sample 83, gabbro suite, is a fine-grained anorthosite, with an average grain-size of 0·2 mm, and a few larger plagioclase grains of up to 4 mm. It has sparse pyroxene and olivine crystals to ~5 mm. Both mafic phases are poikilitic and occur almost entirely in bands with thicknesses of a few centimetres. In these bands, olivine and pyroxene are equally abundant, and make up ~50% of the mode. Scarce clinopyroxene oikocrysts are seen in the anorthositic bands. Olivine is even more rare outside the mafic bands. On outcrop-scale, the mafic bands constitute ~20% of the volume, the rest being anorthosite. The analysed sample represents one of the mafic bands.

Sample 1610 (16xx), wehrlite suite, is from a feldspathic wehrlite plug, emplaced into the LLS (see Bernstein *et al.*, 1992). This plug (at least 30 m × 40 m × 100 m in size) is the most voluminous expression of the wehrlite suite found within the KEHLS. No internal structures have been observed, and the rock has a massive appearance, with ~55–60% olivine, 30–40% green clinopyroxene, 5–15% plagioclase and 5% chrome-spinel. Additionally, ~1–2% anhedral phlogopite crystals are present. The phlogopite usually forms clusters, so that the abundance in thin-section varies widely (1–5%). Olivine, chrome-spinel and phlogopite are fine grained (0·5–1 mm), whereas the pyroxene and subordinate plagioclase oikocrysts are coarser (10–40 mm). The chadacrysts are subhedral olivine and chromite, and the latter phase also occurs as inclusions in olivine. The pyroxene oikocrysts are sometimes zoned, but not as strongly as in sample 61. With *mg*-number in clinopyroxene up to 88, the plug is the most primitive representative of the wehrlite suite. The high modal content of olivine, and the bulk-rock chemistry (>32 wt % MgO) suggest that the wehrlite is olivine accumulative.

Sample 75 (PCT 75), wehrlite suite, is the only representative of the wehrlite suite from the MLS in this study. It intrudes medium-grained ol gabbros, and forms a large (up to 2 km long, and 2–20 m thick) sill-like body [see description by Tegner & Wilson (1993)]. Contact relations to the host gabbros are complex, with remarkable replacement structures bearing evidence of reaction between the host gabbro and melt emerging from the wehrlite sill (Tegner & Wilson, 1993). The analysed sample belongs to the intrusive part of the sill and has a modal composition of 50% olivine, 30% clinopyroxene, 15% plagioclase and 5% oxide. Like all other members of the wehrlite suite, it has phlogopite crystals (~1%) and poikilitic clinopyroxene, enclosing olivine, chromite and plagioclase grains. With clinopyroxene *mg*-number of ~80, the sample is among the most primitive of the wehrlite sills.

Sample SD, wehrlite suite, comes from the western part of the KEHLS, and is a 1 m thick sill, with sharp contacts to the host layered ol gabbros. It is coarse grained, with typical grain-size of 5–8 mm. Poikilitic texture is not so well developed as in most other examples of the suite, and this sample has relatively evolved mineral compositions (*mg*-number is 73–76 in clinopyroxene). The mode is 45% clinopyroxene, 30% olivine, 25% plagioclase and sparse mica. This sample is a melanocratic gabbro, but to avoid confusion about the distinction between the gabbro and the wehrlite suites, all sills belonging to the latter suite will be referred to as 'wehrlites'.

Sample WW, wehrlite suite, ~800 m west of sample SD, represents a thick (4 m) sill which can be followed for almost 1 km along strike, with little change in thickness and in stratigraphic position. It intrudes some well-layered and laminated ol and oxide gabbros, which resemble the oxide gabbros of samples 37 and 38. Large (10–20 mm) clinopyroxene oikocrysts dominate the texture, which in general is very similar to that of the wehrlite plug sample 1610. The modal proportions are 50% olivine, 35% clinopyroxene and 15% plagioclase. In addition to a few percent phlogopite crystals, euhedral amphibole crystals to 2 mm are sporadically present. The *mg*-number of clinopyroxene is 76–77.

Sample 57 (57xx), wehrlite suite, which is a coarse-grained melanogabbro, represents a sill of 1–2 m thickness at the 1320 m stratigraphic level in the LLS (see Bernstein *et al.*, 1992). The sill has poorly defined borders, and along strike the sill seems to disappear into a mafic mixing–mingling zone. Compared with other members of the wehrlite suite, and with many of the host gabbros, this sill has rather evolved mineral compositions, with *mg*-number of clinopyroxene of between 74 and 77. The texture of sample 57 resembles that of sample WW.

Sample 44, wehrlite suite, comes from the LLS, ~20 m stratigraphically above sample 64 (from the gabbro suite). It is a melanocratic sill of 2 m thickness, whose upper contact grades into the host gabbros over a few tens of centimetres. The texture resembles that of most ol gabbros from the gabbro suite, with subhedral clinopyroxenes and olivine crystals of 2–3 mm and plagioclase mostly forming elongated crystals in the interstices. A few of the clinopyroxene grains are optically zoned, in a sector-like fashion. The modal proportions are 40% clinopyroxene, 30% olivine and 25–30% plagioclase. Phlogopite and amphibole together make up ~5% of the mode. Clinopyroxene *mg*-number is 78–81, which makes sample 44 among the more primitive members of the wehrlite sills.

ANALYTICAL TECHNIQUES

To evaluate the composition of the liquids from which the gabbro and the wehrlite suite crystallized, an ion microprobe study was performed on clinopyroxenes from the sample suite described above. The ion microprobe allows high-precision analyses of individual clinopyroxene domains, and is therefore ideal for the study of zoned mineral grains. The analyses were conducted on gold-coated thin-sections with the Cameca IMS-3f ion microprobe at the Woods Hole Oceanographic Institution, using a beam of negatively charged oxygen ions. The trace elements with relatively low atomic numbers—Ti, Cr, V, Sr, Y and Zr—were measured in one sequence, with the following primary beam characteristics: current of 0·2 nA, energy of ~12·6 keV and beam diameter of 5–8 μm. The rare earth elements (REE) were measured in a separate sequence, with a primary beam current of ~1–2 nA and a beam diameter of 12–15 μm. The secondary ion accelerating voltage was reduced by −90 eV for the first sequence of elements, and by −40 to −60 eV for the REE (see Shimizu *et al.*, 1978). The intensities of the following isotopes were measured: ^{28}Si, ^{47}Ti, ^{51}V, ^{52}Cr, ^{88}Sr, ^{89}Y, ^{90}Zr, ^{139}La, ^{140}Ce, ^{146}Nd, ^{147}Sm, ^{151}Eu, ^{163}Dy, ^{166}Er, ^{174}Yb. These secondary ion intensities were then related to concentrations by empirical working curves. The precision and accuracy of the analyses are usually within ±5% for the more abundant trace-elements, and ±10% for the REEs (see also Table 2). The accuracy was monitored by repeated routine analyses of the clinopyroxene standard KH-1.

As the data are acquired in two sequences, it is not possible to analyse all elements in exactly the same spot. This is because the primary beam erodes a deep hole in the sample material (typically 20 μm deep, when measuring the REEs over a 30 min period), which can affect the ionization of the sample material, besides the fact that most thin-sections are only ~25 μm thick. Therefore the two sequences require two separate analysis areas. This obviously presents a problem when analysing heterogeneous material such as strongly zoned clinopyroxene crystals. To circumvent this problem, variations in trace-element data are generally only compared when the elements of interest were acquired from the same analysis sequence. However, some clinopyroxene cores appear homogeneous so that REE and other trace elements can be compared. The number of analyses per sample ranges from two to 12, dependent on degree of zoning.

Major-element concentrations were obtained by electron microprobe analyses at the Geological Institute, University of Copenhagen.

TRACE-ELEMENT DISTRIBUTION IN CLINOPYROXENE

Representative trace-element analyses of clinopyroxenes are given in Table 2. The variation in trace-element concentrations in clinopyroxene from individual samples is very large. This is particularly the case with sample 61. Before calculated liquid compositions are evaluated, the trace-element variation in this sample will therefore be described.

In Fig. 4, analyses of sample 61 clinopyroxenes are presented. The overall patterns show positive correlations between Nd and Nd/Yb, Zr and Sr, and negative correlation between Zr and *mg*-number [molar Mg/(Mg+Fe)], and between Zr and Cr. Individual crystals of sample 61 have variation trends similar to the overall pattern. Cores of clinopyroxene crystals from sample 61 appear to define a group with restricted ranges in trace-element contents. The cores with the highest *mg*-number and Cr content also have the lowest concentrations of incompatible elements (e.g. Zr and Sr) and low Nd/Yb ratios. The distinct chemistry of the clinopyroxene cores versus the rims in sample 61 is also displayed by the variation in major and minor element chemistry. In Fig. 5, clinopyroxene compositions of sample 61 are shown, together with clinopyroxenes from the KEHLS rocks (Bernstein *et al.*, 1992). The clinopyroxene cores of sample 61 form a distinct group with significantly higher Al (and Cr) compared with the rims. The bulk of the KEHLS pyroxenes have lower contents of Al, and overlap with the compositions of clinopyroxene rims of sample 61. In terms of trace-elements, the variation patterns expressed by the sample 61 analyses are typical for all members of the gabbro suite, although the remaining samples show smaller range in the parameters described.

The plug and the sills belonging to the wehrlite

Table 2: Representative trace-element analyses of clinopyroxene cores, obtained by ion microprobe

Sample:	37 p2	± rel. %	± abs.	38 p4	± rel. %	± abs.	83 p1	± rel. %	± abs.	80 p1	± rel. %	± abs.
p.p.m.												
La	1·91	2·26	0·04	1·92	7·64	0·15	1·56	5·4	0·08	1·22	15·05	0·18
Ce	6·85	0·54	0·04	6·92	6·7	0·46	5·25	3·13	0·16	4·08	11·16	0·46
Nd	6·22	5·37	0·33	8·68	1·13	0·1	5·20	6·91	0·36	4·09		
Sm	2·54	2·27	0·06	3·21	3·31	0·11	2·14	5·56	0·12	1·73	10·4	0·18
Eu	0·85	1·98	0·02	1·15	1·76	0·02	0·78	6·14	0·05	0·57	7·4	0·04
Dy	3·15			4·12			2·36			1·91	6·75	0·13
Er	1·72	4·89	0·08	2·43	3·33	0·08	1·27	3·04	0·04	1·07	11·29	0·12
Yb	1·66	1·22	0·02	2·22	3·12	0·07	1·38	1·52	0·02	0·94	5·33	0·05
Ti	6080	0·68	41·59	7894	0·79	62·6	6626	0·65	42·87	4364	0·39	17·02
V	436	0·17	0·75	548	1·73	9·46	432	0·93	4·01	264	1·9	5·02
Cr	338	0·85	2·89	718	1·91	13·68	1431·7	0·67	9·55	2424	1·5	36·36
Sr	24·8	2·4	0·6	26·4	2·31	0·61	27·7	1·8	0·5	21·3	1·26	0·27
Y	15·1	1·27	0·19							10·0	1·96	0·2
Zr	24·4	3·61	0·88	36·8	1·16	0·43	30·7	2·78	0·85	17·1	4·86	0·83
Calculated melt compositions												
Nd/Yb	3·11	5·44	0·17	3·24	3·36	0·11	3·12	7·07	0·22	3·61	5·32	0·19
Eu/Eu^*	0·79	9·36	0·07	0·84	7·42	0·06	0·88	20·1	0·18	0·80	28·55	0·23

	64 p1	± rel. %	± abs.	61 p5	± rel. %	± abs.	44 p2	± rel. %	± abs.	57 p2	± rel. %	± abs.
p.p.m.												
La	1·47	8·43	0·12	0·40	8·13	0·03	1·46	6·36	0·09	2·56	6·81	0·17
Ce	4·36	9·14	0·4	1·48	4·1	0·06	5·20	2·08	0·11	10·15	3·07	0·31
Nd	4·45			1·53	1·18	0·02	4·41	2·55	0·11	10·14		
Sm	2·10	6·97	0·15	0·67	2·03	0·01	2·38	14·78	0·35	3·92	5·33	0·21
Eu	0·71	16·7	0·12	0·31	11·13	0·03	0·65	3·43	0·02	0·99	7·03	0·07
Dy	2·01	11·41	0·23	0·86			2·19			4·59	3·95	0·18
Er	1·23	11·23	0·14	0·50	6·37	0·03	1·21	8·49	0·1	2·56	5·79	0·15
Yb	1·20	17·1	0·2	0·51	11·92	0·06	0·91	12·82	0·12	1·98	3·54	0·07
Ti	4393	0·81	35·58	1851	0·4	7·48	4824	0·69	33·29	6612	0·48	31·54
V	378	1·82	6·88	217	2·65	5·76	365	0·7	2·56	346	0·6	2·08
Cr	2931	1·01	29·6	7538	0·66	50·05	3700	0·96	35·52	127	4·7	5·97
Sr	19·5	1·42	0·28	14·8	5·98	0·89	20·4	2·76	0·56	28	1·81	0·51
Y	10·5	1·62	0·17	4·50	5·86	0·26	13·3	2·48	0·33	22·6	1·27	0·29
Zr	16·3	1·61	0·26	7·10	3·5	0·25	20·9	2·92	0·61	32·8	1·03	0·34
Calculated melt compositions												
Nd/Yb	3·07	16·67	0·51	2·49	11·84	0·29	4·02	13·42	0·54	4·24	3·54	0·15
Eu/Eu^*	0·84	52·95	0·44	1·08	29·99	0·33	0·68	30·6	0·21	0·60	23·75	0·14

(contined on next page)

Table 2: continued

	SD p1	± rel. %	± abs.	WW p1	± rel. %	± abs.	1610 p6	± rel. %	± abs.	75 p2	± rel. %	± abs.
p.p.m.												
La	1·82	5·86	0·11	2·82	7·13	0·2	0·81	8·9	0·07	1·50	2	0·03
Ce	6·23	5·35	0·33	10·62	8·03	0·85	3·11	3·8	0·12	5·26	5·7	0·3
Nd	6·04	3·56	0·22	11·3	7·14	0·81	2·88	11	0·32	5·26	3·6	0·19
Sm	2·61	7·04	0·18	3·99	3·54	0·14	1·01	10	0·1	2·15	10	0·22
Eu	0·80	7·77	0·06	1·21	3·45	0·04	0·39	8·3	0·03	0·76	2·4	0·02
Dy	2·88			4·94			0·89			2·57		
Er	1·57	5·89	0·09	2·74	3·97	0·11	0·47	15	0·07	1·21	4·1	0·05
Yb	1·25	3·38	0·04	2·30	2·69	0·06	0·38	4·4	0·02	1·09	7·8	0·09
Ti	5686	0·66	37·53	6369	0·95	60·19	2810	2·16	60·7	5368	1·9	102
V	361	1·07	3·86	329	0·87	2·86	227	3·05	6·92	355	4·5	15·98
Cr	2354	0·25	5·89	895	1·17	10·47	7981	0·29	23·14	5310	2·4	127·4
Sr	23·2	2·36	0·55	23	1·09	0·25	36	4·13	1·49	25	4·2	1·05
Y	14·8	3·86	0·57				7·1	3·03	0·22	11·9	4·3	0·51
Zr	25	6·11	1·53	44	2·01	0·88	9·2	3·97	0·37	22	11	2·42
Calculated melt compositions												
Nd/Yb	4·00	4·85	0·19	4·07	7·63	0·31	6·28	12·29	0·77	4·00	9·01	0·36
Eu/Eu*	0·74	25·08	0·19	0·72	11·79	0·08	0·97	29·2	0·28	0·84	15·26	0·13

Nd/Yb and Eu/Eu* are chondrite-normalized, calculated melt compositions in equilibrium with clinopyroxene. Eu/Eu* = Eu/[2(Sm+Dy)/3].

suite exhibit variation patterns different from those of the gabbro suite. The most primitive representative of the wehrlite suite, the wehrlite plug sample 1610, shows a complex pattern of variation (Fig. 6). Some of the trends are opposite to those of the gabbro suite. This is the case with the Nd/Yb vs Nd diagram, where a weak, negative correlation exists. Negative correlations are also evident in the Eu/Eu* vs Nd and Cr vs Zr diagrams. The wehrlite sills roughly mimic the trends defined by the wehrlite plug. This is especially the case in the REE variation diagrams. The wehrlite sill samples 44 and 75 show large variations in Nd/Yb within a narrow range in Nd concentration. If any correlation can be detected, it would be a tendency for lower values of Nd/Yb with increasing Nd content (sample 57). Similarly, for samples 44 and 75 the variation in Eu/Eu* is large and correlates poorly with Nd. As is true for the Nd/Yb vs Nd plot, samples 57, WW and SD define weak negative trends between Eu/Eu* and Nd. In the plot of Sr vs Zr, a similar pattern is seen, with a more marked tendency for Sr to decrease with increasing Zr (samples WW, SD and 57). Compared with the wehrlite plug, all sill members of the wehrlite suite have low Nd/Yb, lower concentrations of Sr and Cr, and more pronounced negative Eu anomalies.

DISCUSSION

In general, the analysed clinopyroxene crystals from the gabbro suite show normal zoning patterns, with negative correlation between compatible and incompatible elements. Similar zoning of major elements in clinopyroxene from the MLS has been demonstrated by Tegner & Wilson (1995). This type of zoning is in contrast with the studies of clinopyroxene phenocrysts in basalts by Shimizu (1981), Shimizu & LeRoex (1986) and Vannucci *et al.* (1993), and suggests that disequilibrium crystallization played only a minor role in developing the trace-element patterns described above. For the gabbro suite samples, as exemplified by sample 61 (Fig. 4), the trace-element patterns can be explained in terms of fractional crystallization (see Fig. 12, below, for other gabbro suite samples). The increase in LREE to HREE ratio (Nd/Yb) and strong decrease in chromium can be caused by clinopyr-

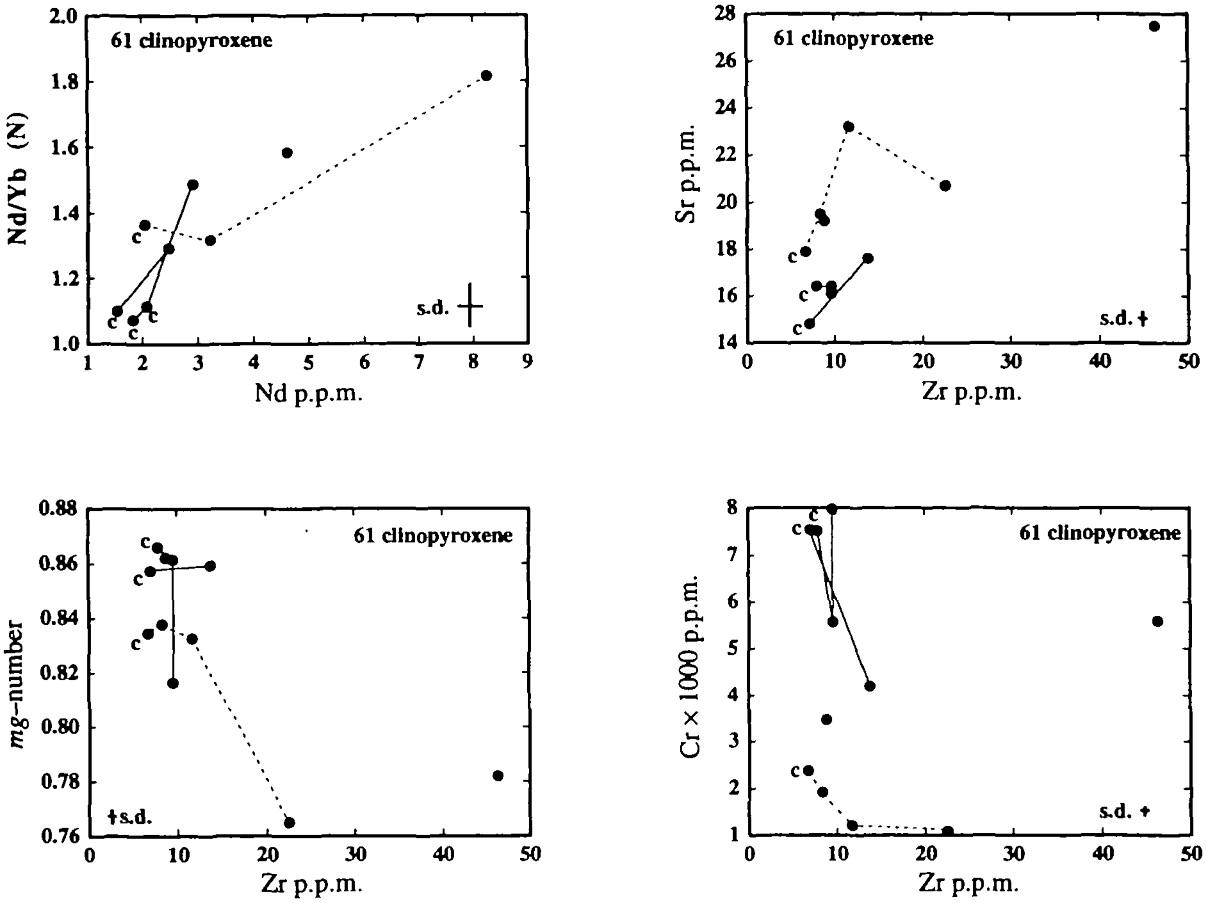

Fig. 4. Chemical variation diagrams for compositions of clinopyroxenes from melanocratic sill sample 61 (gabbro suite). Nd/Yb is chondrite normalized (Sun & McDonough, 1989). Analyses from individual crystals are linked, and (c) is crystal core analysis. Crystal (a) referred to in text is marked with a dashed line. Average analytical error is given by the bars in the corner of each diagram.

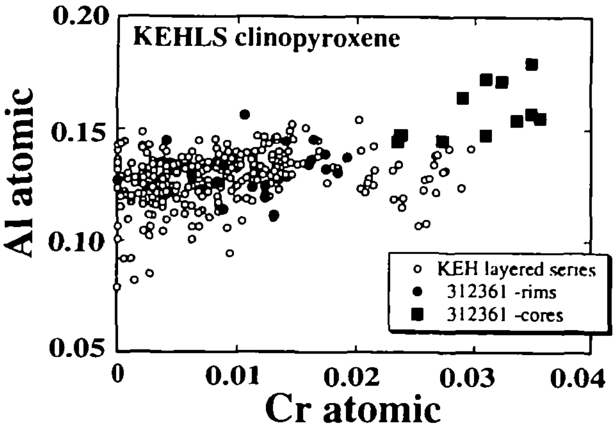

Fig. 5. The compositions of KEHLS clinopyroxenes in terms of aluminium and chromium, expressed as atoms per six oxygen in unit formula. [Note the distinctly higher Al in cores of clinopyroxene from sample 61 (Fig. 3).]

oxene fractionation, which, together with olivine fractionation, also accounts for the decrease in *mg*-number with increasing Zr content. The general increase of Sr with increasing Zr points towards suppressed plagioclase fractionation, because the high proportion of plagioclase (~50%) in the fractionating solid assemblage along the low-pressure cotectics will result in a bulk partitioning coefficient close to unity for Sr (given the high partition coefficient for Sr in plagioclase; Table 3). Crystal 'a' in Fig. 4 may thus record the early crystallization of clinopyroxene (+olivine) which results in increasing Nd/Yb ratios, strong depletion in Cr, and a positive correlation between Zr and Sr. The break in the Sr–Zr curve (at ~12 p.p.m. Zr) would then record the onset of plagioclase fractionation.

Similarly, for the wehrlite plug (sample 1610; Fig. 6), the positive trend in Sr–Zr, followed by a

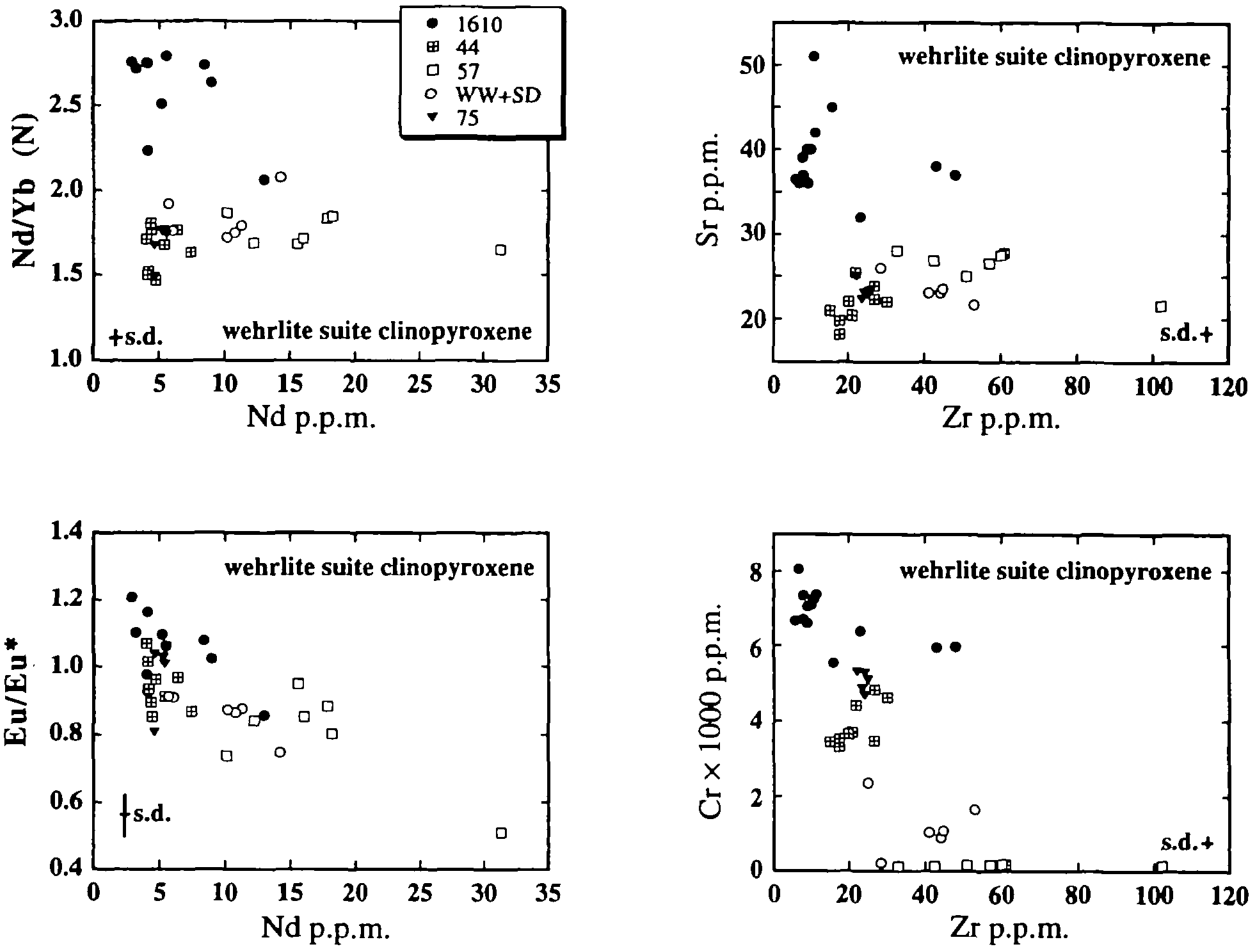

Fig. 6. Variation in trace-element chemistry of clinopyroxene from the wehrlite suite. The clinopyroxene from the wehrlite sills has consistently lower Nd/Yb ratios, Sr and Cr contents compared with the clinopyroxene of the wehrlite plug sample 1610. Average error bars are given in each diagram.

Table 3: Partition coefficients for solid phases–melt

	Ca-pyroxene	Ref.	Plagioclase	Ref.	Olivine	Ref.	Fe–Ti oxide	Ref.
La	0·05	1	0·16	4	0·00001	9	0·006	8
Ce	0·09	1	0·15	4	0·00001	9	0·006	8
Nd	0·19	1	0·14	4	0·00007	9	0·008	8
Sm	0·29	1	0·12	4	0·0007	9	0·01	8
Eu	0·3	2	0·68	5	0·0009	9		
Dy	0·44	1	0·08	4	0·004	9	0·02	8
Er	0·39	1	0·08	4	0·009	9	0·03	8
Yb	0·43	1	0·07	4	0·023	9	0·05	8
Ti	0·38	1	0·05	6	0·015	9	12	12
Cr	10 (3·8)	3 (1)	0·02	7	1	10	60	12
Sr	0·13	1	2	4	0·003	6	0·7	12
Y	0·47	1	0·03	4	0·02	11	0·04	11
Zr	0·12	1	0·01	8	0·01	8	8	12

References: 1, Hart & Dunn (1993); 2, McKay (1989); 3, Barnes (1986); 4, Drake & Weill (1975); 5, Paster *et al.* (1974); 6, Irving (1978) and references therein; 7, Sun *et al.* (1979); 8, Fujimaki *et al.* (1984); 9, Kelemen *et al.* (1992); 10, Lemarchand *et al.* (1987); 11, by analogy with Er and Yb; 12, Villemant *et al.* (1981).

negative trend, may be explained by clinopyroxene–olivine fractionation followed by plagioclase fractionation. The decrease in Eu/Eu* and Sr with increasing Nd and Zr observed for the samples 57, WW and SD may likewise reflect crystallization of a plagioclase-rich solid assemblage. It should be noted that these three samples also are the most evolved in terms of *mg*-number and Cr content (Table 1 and Fig. 6). In contrast, the large variations in Nd/Yb, Eu/Eu* and Sr within very restricted Nd and Zr contents, especially in samples 44 and 75, suggest that the pyroxenes crystallized from heterogeneous melts, which are not related by simple fractional crystallization. The heterogeneity may rise from magma mixing or metasomatic processes, and will be discussed below.

For the studied samples, it appears that most of the variations in trace-elements can be qualitatively related to crystal fractionation, and that the fractionating assemblage, according to the variation patterns, is olivine/clinopyroxene followed by olivine/plagioclase–clinopyroxene. Even though the oikocrystic state of many of the analysed clinopyroxene crystals conventionally is taken as evidence of late growth of clinopyroxene, the positive correlation in the Sr–Zr diagram argues against significant plagioclase fractionation before or during the early growth of the clinopyroxene. Early crystallization of clinopyroxene is also suggested by the increase in Nd/Yb at low contents of Nd for most samples (see also Fig. 12, below). This is because clinopyroxene is the only plausible phase during crystallization of tholeiitic melt (at pressures below garnet stability) that has sufficiently high partition coefficients for the heavy REE to fractionate Nd from Yb. The increase in Nd/Yb seen in, for example, Fig. 4 would therefore be difficult to obtain with low-pressure 'gabbro' fractionation because of its low proportion of clinopyroxene in the fractionate (~35%). A similar conclusion of early clinopyroxene growth in cumulates was also reached by Tegner & Wilson (1995) on the basis of major element variations in clinopyroxene oikocrysts from the MLS. The sequential crystallization (olivine/clinopyroxene joined later by plagioclase) suggested by the trace-element distributions described above is in agreement with the work of Kirkpatrick (1977, 1983) and Brandeis *et al.* (1984). They demonstrated that plagioclase, because of its higher polymerization state, has higher nucleation energy, and therefore requires higher degrees of undercooling to reach maximum growth rate than do the ferro-magnesian minerals olivine and clinopyroxene, which have simpler structures.

Composition of equilibrium melts

Because it appears that clinopyroxene preceded substantial plagioclase growth in all samples considered, only olivine and chrome-spinel fractionation may have affected the melt composition before saturation of clinopyroxene was reached. Owing to their very low partition coefficients for the trace-elements considered, any early fractionation of olivine and chrome-spinel must have played a negligible role (except for Cr) in the characteristics of the trace-element composition of the parental melt, considering the range of variability observed. Therefore, for a given sample, the calculated equilibrium melt composition based on the 'least evolved' clinopyroxene analysis in each sample is believed to be representative of the parental melt. The 'least evolved' analysis refers to the lowest recorded concentration of the incompatible elements REE and Zr in each sample. The selection is based on the assumption that none of the observed cumulus phase assemblages has a bulk partition coefficient higher than unity for the REEs or Zr. The 'least evolved' analysis is taken as the closest approximation to the values in equilibrium with the melt from which the first clinopyroxene crystallized. Trace-element concentrations in equilibrium liquids are then calculated using published partition coefficients (Table 3). The partition coefficients used are determined in basaltic systems with limited *mg*-number, and are assumed insensitive to variations in intensive parameters during the crystallization processes considered in this study. This is substantiated by the high-pressure experimental work of Hart & Dunn (1993), whose partition coefficients are adopted here, and whose results do not differ markedly from those obtained at low pressures by, for example, Gallahan & Nielsen (1992).

The melt compositions calculated in this way are shown in the chemical variation diagrams of Fig. 7. The gabbro and the wehrlite suites define two coherent groups with the following characteristics. The gabbro suite shows positive correlation between Nd/Yb and Nd, and a strong positive correlation between Sr and Zr. Sample 61 has a weak positive Eu anomaly, whereas the remaining samples of the gabbro suite cluster at a negative Eu anomaly of ~0·8. Finally, Cr shows strong negative correlation with Zr. As for sample 61 from the gabbro suite, sample 1610 defines the primitive end of the more complex trends of the wehrlite suite. Apart from sample 1610 from the wehrlite plug, the wehrlite sill samples define trends sub-parallel to those of the evolved gabbro suite samples. Generally, the wehrlite suite has higher Nd/Yb ratios and higher Zr

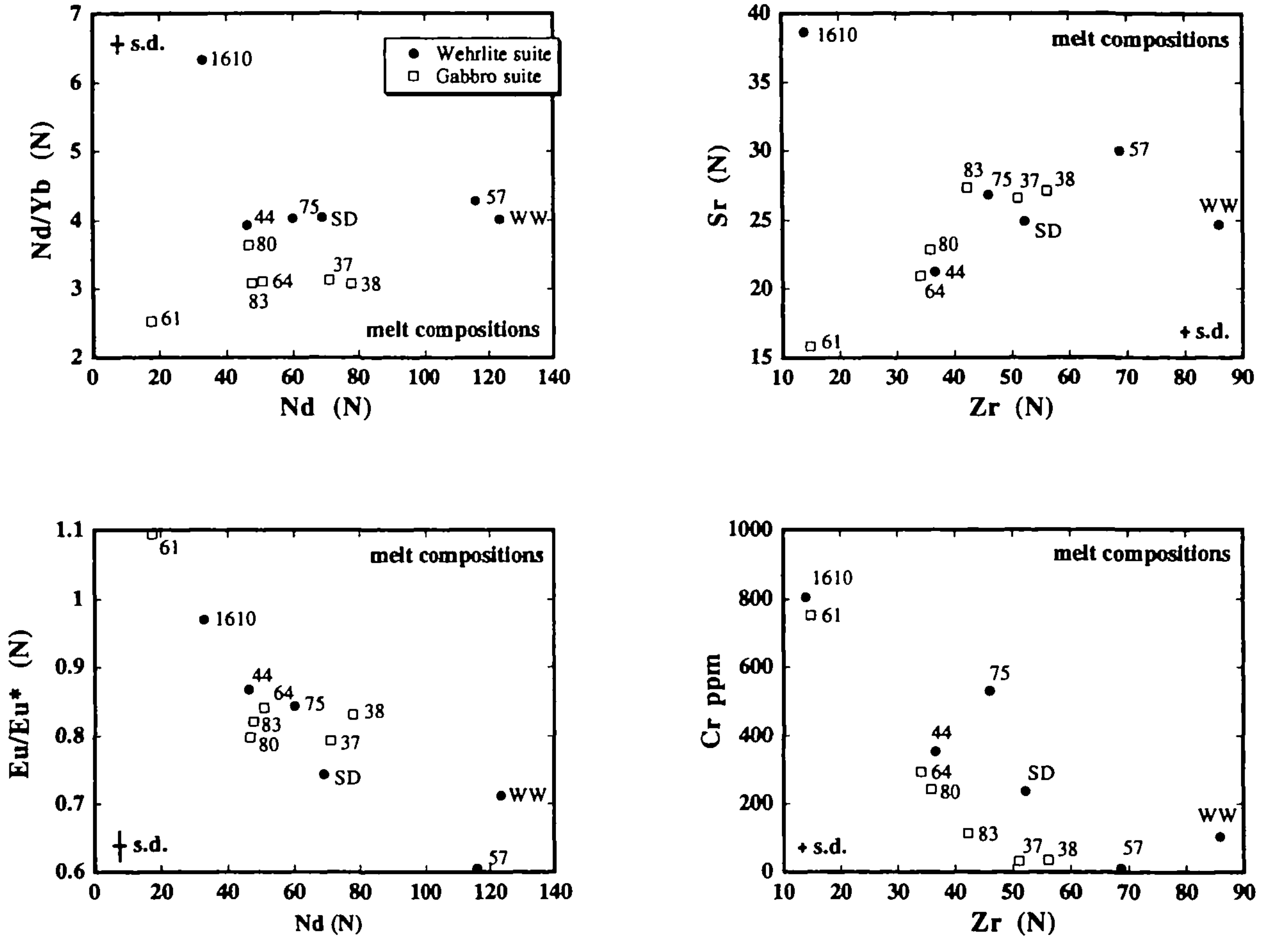

Fig. 7. Compositions of melts in equilibrium with the analysed samples, computed from 'least evolved analyses' (see text) using the partition coefficients listed in Table 3. The two primitive end-member melt compositions 61 and 1610 for the gabbro and wehrlite suite, respectively, have strongly contrasting Nd/Yb ratios and Sr contents. The sills of the wehrlite suite show compositions roughly parallel to those of the gabbro suite melts, although somewhat displaced towards higher Nd/Yb. Average error bars are given in each diagram.

contents than the gabbro suite for a given Nd or Cr concentration. The overall range in trace-element concentrations is larger for the wehrlite suite. This becomes especially evident when comparing the wehrlite sills with the evolved gabbros.

Crystallization models

The evaluation of crystallization processes below should be seen in the light of the sample collection that forms the basis of this work. There is little knowledge of the time difference between the formation of individual lithologies, although they were all formed during the supersolidus stage of the KEHLS magma chamber. Furthermore, because of the relatively few samples in this study, compared with traditional basalt studies, our modelling should be considered in mainly qualitative terms.

The primitive end of the gabbro suite is defined by sample 61, which is chosen as the closest approximation to the melt parental to the gabbro suite. This seems justified by the observations that the sample 61 calculated liquid has low chondrite-normalized abundances of incompatible elements, unfractionated REE patterns, Cr concentrations in the range of primitive MORB (Wilson, 1989), and that the clinopyroxene cores have *mg*-number of ~90, which is in the range expected for clinopyroxene in equilibrium with a primary, mantle-derived melt. Various crystallization models have been conducted to evaluate how the evolved liquid members of the gabbro suite relate to the primitive liquid sample 61. The modelling has been performed on the elements listed in Table 2, with the solid–liquid partition coefficients in Table 3, using the Rayleigh equation $C_l = C_0F^{(D-1)}$, where C_l and C_0 are concentrations of an element in fractionated and initial melt respectively, F is residual melt fraction and D is bulk partition coefficient.

Rayleigh fractionation at low pressures

For low-pressure fractional crystallization of a tholeiitic basalt, the proportions of plagioclase–clinopyroxene–olivine are approximately 0·50–0·30–0·20, respectively (Biggar, 1983; Komor *et al.*, 1987; Grove *et al.*, 1992). These proportions are broadly consistent with the cumulus assemblage and modal abundance observed in the KEHLS gabbros (Bernstein *et al.*, 1992). To produce the Nd concentration of the intermediate melts (e.g. sample 83) from sample 61, 65–70% fractional crystallization is required, using the low-pressure fractionation assemblage in the proportions listed above. The resulting liquids (see fractionation paths 'LP frac.' in Fig. 8) develop negative Eu anomalies (low Eu/Eu* ratios), that correspond well to the values of the intermediate gabbros. Also, Zr and Cr concentrations are modelled satisfactorily (Fig. 8). However, Nd/Yb ratios and Sr concentrations are not in accordance with observed values. During low-pressure fractionation, Nd/Yb ratios and Sr concentrations of residual liquids are nearly constant, reflecting the high proportion of plagioclase in the cumulus assemblage [with a high partition coefficient (D) for Sr and high D_{Nd}/D_{Yb}]. The positive correlation between Sr and Zr may be explained in terms of early olivine fractionation, but the intermediate samples 64, 80 and 83 have *mg*-numbers that are too low (clinopyroxene *mg*-number 78–80) to have only olivine on their liquidi. More importantly, olivine is not capable of fractionating the REE sufficiently, and it is not likely that olivine fractionation alone can dominate for up to 65% crystallization, which is needed to account for the variations in Nd and Zr concentrations by fractionation. Application of a more complex fractionation model involving replenishments, tapping and continuous fractional crystallization (RTF; O'Hara & Mathews, 1981; see below) does not change the overall pattern outlined by simple fractional crystallization. It can therefore be stated that fractional crystallization involving the phase proportions appropriate for crystallization of a tholeiitic melt at low pressure cannot produce the trace-element pattern observed for the gabbro suite. Crystallization at higher pressures is therefore evaluated below.

The effect of pressure on the proportions of crystallizing phases

The cotectic proportions of the phases plagioclase, clinopyroxene and olivine change progressively with increasing pressure towards higher clinopyroxene proportions relative to the other two phases (e.g. Bender *et al.*, 1978; Presnall *et al.*, 1978; Fujii & Bougault, 1983). In high-pressure experiments on mildly alkaline basalts from Surtsey, Iceland (10–12·5 kbar), the phase proportions of plagioclase, clinopyroxene and olivine are roughly 0·18–0·47–0·35 (Thy, 1991), and 10 kbar experiments on a synthetic high magnesium tholeiite yielded the plag–cpx–ol proportions of 0·13–0·55–0·32 (Grove *et al.*, 1992), highlighting the importance of clinopyroxene in the crystallizing assemblage at higher pressures. In addition, Furman *et al.* (1991) successfully modelled a suite of Surtsey lavas using an inferred 10 kbar crystallizing assemblage plagioclase, clinopyroxene and olivine of roughly 0·20–0·51–0·29. In the following, the proportions plag–cpx–ol 0·20–0·50–0·30 have therefore been employed in describing the effects of fractional crystallization at deep crustal levels, i.e. at pressures of ~10–12 kbar.

Rayleigh fractionation at high pressures

Simple fractional crystallization of the high-pressure cumulus assemblage yields a somewhat better match to some of the observed trends (trend 'HP frac.' in Fig. 8). The amount of fractionation to produce the Nd concentration of sample 83 from the primitive sample 61 melt is again 65–70%, and the high proportion of clinopyroxene in the fractionate has a significant effect on the Nd/Yb ratio, compared with the low-pressure fractionation. The suppressed plagioclase fractionation results in strong positive correlation between Sr and Zr, duplicating the observed gabbro suite fairly well. However, the low plagioclase proportion also results in much less depletion in Eu with fractionation, so that the model Eu/Eu* trend differs markedly from the observed gabbro suite. Another problem arises from the strong depletion of Cr in the 10 kbar model, which is due to the high clinopyroxene proportion in the fractionate. Rayleigh fractionation of 65–70% leaves only a few p.p.m. Cr in the residual melt. Similarly, calculated melts of the samples 83, 80 and 64 have *mg*-number of 48–50, in apparent contradiction to the high fractionation degrees inferred from the incompatible element enrichment. If the initial sample 61 melt with *mg*-number of 69 is assumed to have FeO + MgO of ~21 wt %, which is typical for Tertiary basalts from Greenland (Pedersen, 1985; Larsen *et al.*, 1989), the evolved melt, after some 65–70% Rayleigh fractionation, will have *mg*-number of ~32 (Fig. 9). Although it is noted that some of the patterns of the chemical variations in the gabbroic suite point towards the characteristics of high-

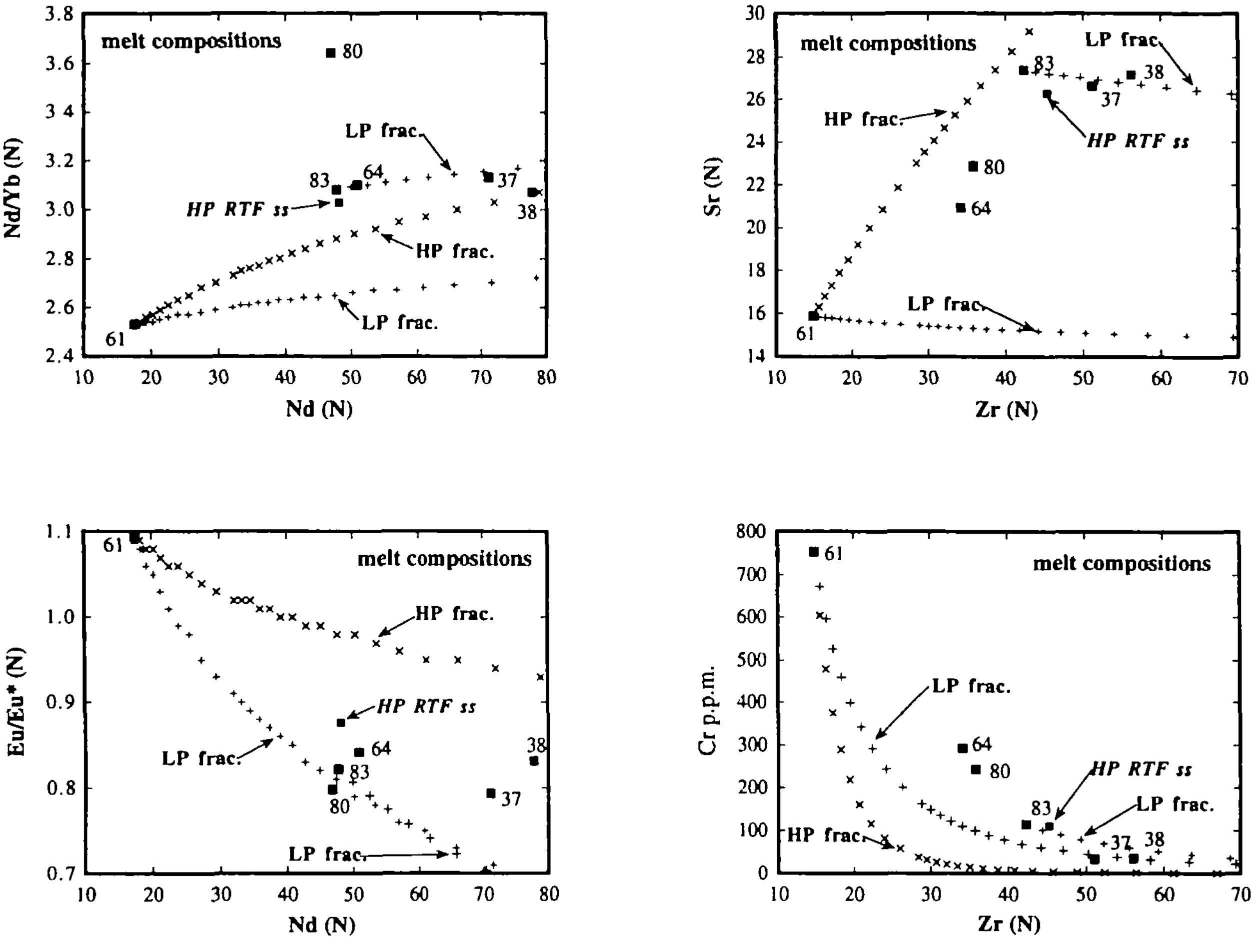

Fig. 8. Compositional variations in melts from the gabbro suite. The two trends 'LP frac.' show low-pressure Rayleigh fractionation of the assemblage 0·5plag–0·3cpx–0·2ol with sample 61 as parental liquid, and the assemblage 0·5plag–0·3cpx–0·18ol–0·02FeTi oxide with sample 83 as parental liquid. 'HP frac.' stands for high-pressure fractionation of the assemblage 0·2plag–0·5cpx–0·3ol with sample 61 as parental liquid. 'HP RTF ss' is the steady-state product of high-pressure RTF processes (see text for details). Crosses depict Rayleigh fractionation of the phase assemblage stated above in 5% increments for $1{\cdot}0 > F > 0{\cdot}5$, and 2% increments for $0{\cdot}5 > F$.

pressure fractionation (Nd/Yb vs Nd, and Sr vs Zr), it must be concluded that a simple Rayleigh fractionation model is insufficient to describe the observed trends. Two other possibilities exist, which will be evaluated below: (1) mixing processes between a melt of sample 61 composition and melts with contrasting chemical characteristics, or (2) involvement of RTF (replenishment, tapping and fractionation) processes.

The gabbroic suite as a product of mixing processes

With the evidence of co-magmatism of the wehrlite and the gabbro suites (Bernstein *et al.*, 1992; Tegner *et al.*, 1993), mixing between the two suites is an obvious possibility. The wehrlite suite mixing end-member is taken as the sample 1610, because the wehrlite sills are regarded as being mixing products themselves (see the section below) and not fractionation products of the primitive sample 1610 melt. The field evidence suggests that the wehrlite sills intruded the solidifying gabbros, i.e. during the cooling stage of the magma chamber, but this observation does not rule out that the two liquid suites could have coexisted throughout the lifetime of the KEHLS magma chamber. Two mixing processes can be envisaged; the first is injection of sample 1610 melt into the magma chamber, where it hybridizes with the residing magmas undergoing low-pressure fractionation. This process, however, is incapable of affecting the REE budget sufficiently because the wehrlite suite volumetrically makes up <1%.

The second process is mixing between the sample 61 and 1610 melts followed by injection of the

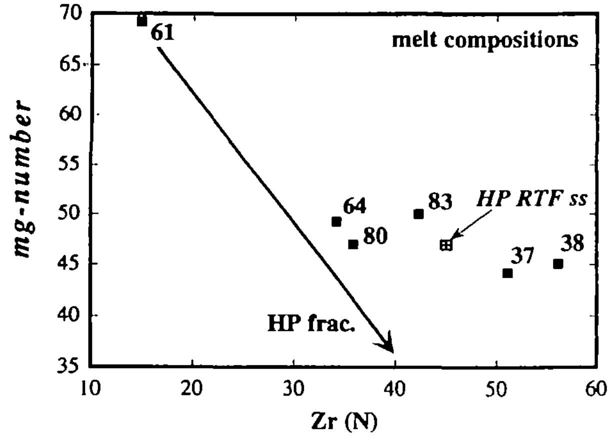

Fig. 9. The *mg*-number and Zr concentrations in melts calculated in equilibrium with clinopyroxene cores of the gabbro suite, based on K_d (*mg*-number liquid/*mg*-number cpx)=0·25 (see text). Simple Rayleigh fractionation leads to a depletion in *mg*-number outside that observed in the KEHLS gabbros (arrow labelled HP 'gabbro' fractionation), whereas RTF process ('HP RTF ss'), with the parameters estimated in the text, accounts more satisfactorily for the observed values. The Rayleigh fractionation model used the bulk partition coefficients and starting liquid composition described in the text.

resulting hybrid magma into the KEHLS magma chamber, where the magma subsequently underwent low-pressure fractionation. The chemical consequence of this mixing process is outlined in Fig. 10. It is evident that large amounts of 'wehrlite' magma are required to mix with the sample 61 magma to approach the values of the gabbro suite in terms of Nd/Yb ratios and Sr concentrations. Apart from sample 80, the combined mixing and fractionation curves fit the Sr concentrations in the gabbro suite poorly (Fig. 10). It is thus unlikely that the chemical trend of the gabbroic suite is solely due to mixing processes, and possibility (2) involving RTF processes will be considered next.

RTF model

In the RTF model (O'Hara & Mathews, 1981), the periodical replenishment, tapping and continuous fractionation results in a steady-state melt composition after a certain number of cycles, provided that the parameters x (amount of fractional crystallization), y (amount of tapping) and z (amount of replenishments) are held constant. The success of the RTF model, which in general is more realistic in describing magma chamber processes than is simple Rayleigh fractionation, has been demonstrated by, for example, Cox (1988), Hogg *et al.* (1988) and Larsen *et al.* (1989). An effect of RTF processes is that incompatible elements with slightly different bulk partition coefficients are fractionated from each other to a greater extent than expected from examining the variations in absolute concentrations. For the major elements that have bulk partition coefficients around unity the RTF process results in very limited variations, so that qualitatively the RTF model may be able to explain the large variation in incompatible elements along with the small range in *mg*-number in clinopyroxenes.

The anorthosite–leucogabbro sample 83 at the basal part of the MLS was chosen to represent the intermediate gabbros, because the field relations and compositional variations suggest that this rock body represents a new injection of fresh magma (Abbott & Deer, 1972; Fehlhaber & Bird, 1991). To assess whether the sample 83 melt composition can be related to the parental melt 61 through RTF processes, an enrichment factor ($r=C_l/C_0$, where C_0 is initial melt concentration, sample 61, and C_l is concentration in evolved melt, sample 83) was determined for the elements listed in Table 4. Also listed are the bulk partition coefficients for the high-pressure assemblage 0·2plag–0·5cpx–0·3ol. The rela-

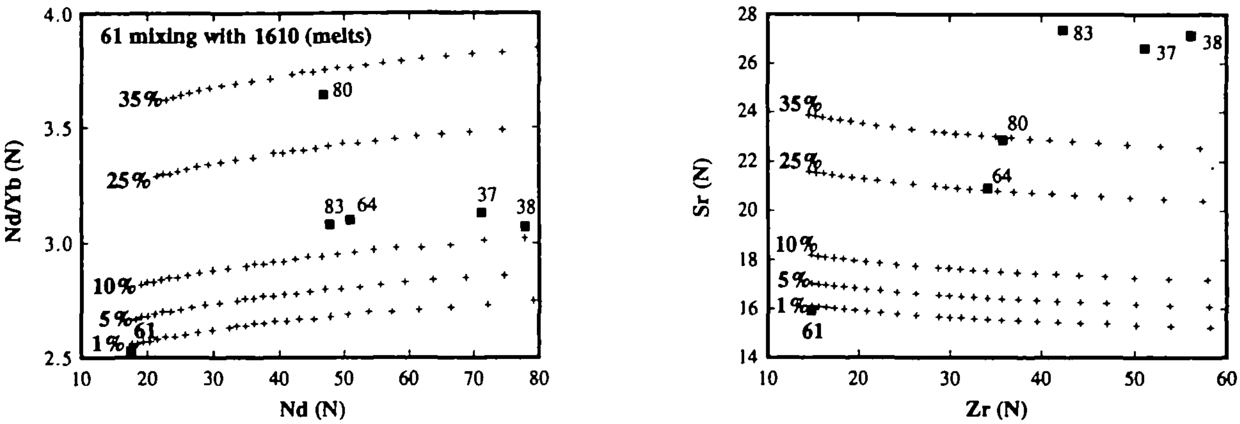

Fig. 10. The result of bulk mixing of sample 61 liquid with 1–35% of sample 1610 liquid, followed by low-pressure Rayleigh fractionation of the assemblage 0·5plag–0·3cpx–0·2ol. Fractionation increments as in Fig. 8.

Table 4: Enrichment factors r, *and bulk partition coefficients* D, *for calculating RTF parameters, assuming that sample 83 is an RTF product of sample 61*

	Nd	Yb	Cr	Sr	Zr
r	2·72	2·23	0·16	1·72	2·84
D	0·122	0·23	5·3	0·474	0·067

Bulk partition coefficients from Table 3, based on the assemblage 0·2 plagioclase–0·5 clinopyroxene–0·3 olivine.

tionship between the concentrations of an element i in the initial melt, $C_{i,0}$, and in the steady state erupted melt, $C_{i,1}$, can be expressed by the equation

$$\frac{C_{i,1}}{C_{i,0}} = r_i = \frac{(x+y)(1-x)^{D_i-1}}{1-(1-x-y)(1-x)^{D_i-1}} \qquad (1)$$

where x and y are defined above (assumed constant), and where D_i is bulk partition coefficient for element i (O'Hara & Mathews, 1981). Solving equation (1) for y yields

$$y = \left[x - xr_i + r_i - \frac{r_i}{(1-x)^{D_i-1}}\right]\frac{1}{1-x}. \qquad (2)$$

The result of equation (2) for the elements in Table 4 is shown in Fig. 11. The near parallelism of the lines for the incompatible elements in Fig. 11 implies that the sample 83 melt may indeed be a product of RTF processes with sample 61 as the parental melt. If the sample 83 melt composition is to be modelled by the RTF model with reasonable accuracy with respect to chromium, x and y must be in the range of 0·16–0·22 and 0·05–0·10, respectively. Furthermore, x/y must be in the range 2·8–3·2, the lower limit arbitrarily set by Nd/Yb in residual melts to be higher than 3·0 and the upper limit defined by contents of Nd and Zr in residual melts to be lower than 55 and 50 times chondrite, respectively (Fig. 8). These values for x and y are similar to results of numerical modelling by Cox (1988) of a sequence of basalts from the Deccan Traps. He found that if RTF were to produce the observed chemical variation, x and y had to attain values larger than 0·05 and 0·04, respectively. The x/y ratio of around three is higher than Cox's estimate ($0·5 < x/y < 1·3$) and results from the higher degree of fractionation required in the model, because of the rather large r values in the present study (Table 4). The erupted steady-state composition resulting from

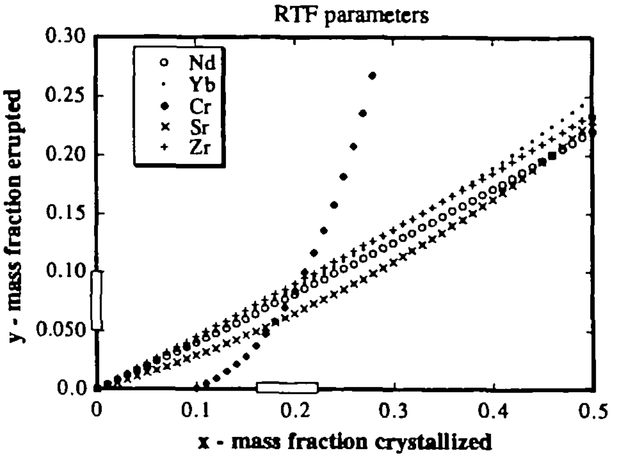

Fig. 11. The RTF parameters x and y, which in addition to the parameters in Table 4 determine the composition of steady-state melt. x and y are calculated from equation (2) in the text. [Note the restricted ranges in x and y to allow the chemical characteristic of sample 83 melt (given by bars on x and y axes).] The parallelism of the curves for the incompatible elements suggests a good fit between the RTF model and the observed elemental distribution in melt 83.

$x = 0·2$ and $y = 0·08$ is presented in Figs 8 and 9 ('HP RTF ss'). As expected, the composition of the 'HP RTF ss' is close to that of sample 83, but not only in terms of the elements considered in Table 4; Eu/Eu* (Fig. 8) and *mg*-number also are better accounted for by the RTF model. In the high-pressure assemblage of 0·2plag–0·5cpx–0·3ol, the bulk partition coefficients of Mg and Fe are 2·2 and 0·7, respectively, calculated on the basis of $K_{D,ol(Mg,Fe)} = 0·33$ (Roeder & Emslie, 1970) and $K_{D,cpx(Mg,Fe)} = 0·25$ (Grove & Bryan, 1983). These bulk partition coefficients are practically identical to those determined by O'Hara (1977). The RTF steady-state melt calculated above will have an *mg*-number of ~48, which is within the range of the melt calculated for the sample 83 clinopyroxene (*mg*-number 48–50). No information on the size of z (amount of incoming parental melt) is given by the above calculations, as the steady-state composition is independent of z. In contrast to studies of basalt series, there are poor constraints on the relative age of individual sequences in intrusions, rendering z impossible to estimate.

For sample 64, it is possible that fluctuations in the x and y parameters and subsequent mixing with low-pressure fractionates residing in the KEHLS magma chamber could give rise to the observed low Sr and Zr, and high Cr concentrations compared with sample 83. For example, when x and y are very small, chromium is depleted very slowly by RTF processes. For sample 80, however, no possible fractionation process (at pressures <15 kbar, i.e.

without garnet fractionation) can account for its high Nd/Yb. The chemistry of this sample may be accounted for by other processes, and it should be noted that from the mixing calculations presented in Fig. 10, it appears that sample 80 may indeed represent mixing between the gabbro and wehrlite suite melts.

Evidence of high-pressure fractionation can be found in the composition of the clinopyroxenes from sample 61. As noted above, some of the large clinopyroxenes have euhedral cores, sometimes partly resorbed, with high *mg*-numbers and Cr contents. These clinopyroxene cores are interpreted as phenocrysts, which formed at the deep-seated RTF magma chamber before emplacement of the sill. As demonstrated in Fig. 5, the rims of the sample 61 clinopyroxenes are indistinguishable from the bulk of the KEHLS gabbro clinopyroxenes, whereas the sample 61 clinopyroxene cores are displaced towards considerably higher aluminium and chromium contents. Numerous experiments and calculations have shown that the solubility of the Ca-tschermak component in clinopyroxene increases with pressure (e.g. Wood, 1976; Herzberg, 1978), so on this basis the high Al content of the euhedral clinopyroxene cores lends further credit to the high-pressure fractionation model.

The liquid, from which the evolved oxide gabbros 37 and 38 crystallized, cannot be directly produced from sample 61 by crystallization at either high or low pressure. The evolved oxide gabbros may be low-pressure fractionates of sample 83 melt, with the assemblage 0·5plag–0·3cpx–0·18ol–0·02FeTi oxide (see Fig. 8). In this way, the 'oxide gabbro' melts may represent some 35% fractionation of melt 83. The Eu contents of the oxide gabbro melts are not readily explained by fractionation of the above assemblage. The high plagioclase content in the fractionate is expected to result in a strong negative Eu anomaly. However, the Eu/Eu* values in the sample 37 and 38 melts are similar to those of the parent melt. A possible explanation could be higher f_{O_2} in the low-pressure KEHLS magma chamber, relative to the high-pressure fractionation magma chamber(s). The partitioning of Eu between plagioclase and liquid is a strong function of the oxygen fugacity, with D_{Eu} varying from ~1·0 at the iron–wüstite buffer to ~0·25 at the quartz–magnetite–fayalite buffer at ~1200°C (McKay *et al.*, 1989). The relative incompatibility of Eu in the low-pressure system could also be due to a negative Eu anomaly in clinopyroxene, as suggested by the study of Morse & Nolan (1985) on the REE systematics of the Kiglapait intrusion. In the present study, the high errors in the determination of Eu/Eu* (Table 2) render these values difficult to constrain.

To summarize, all gabbros more evolved than sample 61 have significantly higher Nd/Yb than sample 61. Also, these gabbros display a strong positive correlation between Zr and Sr. These features are indicative of high proportions of clinopyroxene in the fractionate, and coupled with the mild depletion of chromium when considering the high contents of incompatible elements, suggest that RTF processes at ~10 kbar are responsible for the observed trends. The independent calculation of *mg*-number of the HP RTF ss product using *x* and *y* values derived from the concentrations of trace-elements, and the high Al content of sample 61 clinopyroxene cores, provide arguments in favour of the high-pressure RTF model. Field relations suggest that the leucogabbro–anorthosite sample 83 represents a new influx of melt into the KEHLS magma chamber. The high modal proportions of plagioclase in this rock can hence be explained as a result of preceding fractionation of primitive sample 61 melt at high pressures. In response to the pressure release following transport of the evolved magma from the deep-seated magma chamber to the KEHLS magma chamber at 1–2 kbar, the melt was saturated with plagioclase, and fractionated large amounts of this phase before reaching the low-pressure eutectic plagioclase–clinopyroxene–olivine. The preferred model for the evolution of the KEHLS magma chamber is therefore that it was predominantly fed by magmas evolved at high pressure, which upon injection into the KEHLS magma chamber underwent low-pressure fractionation to form the bulk of the layered olivine and oxide gabbros. Only rarely was a primitive, essentially unfractionated, Mg-rich melt allowed through the plumbing system, in this case forming the melanocratic sill sample 61.

Origin of the wehrlite sills

As mentioned above, and as stressed by Bernstein *et al.* (1992), there is compelling evidence for a genetic link between the wehrlite plug and the wehrlite sills. One of the strongest arguments is the presence of phlogopite crystals in all members of the wehrlite suite, in contrast to the gabbro suite, which is virtually devoid of this phase. The phlogopite crystals in the wehrlite suite are commonly strongly deformed, as described by Bernstein *et al.* (1992). The latter observation suggests that this phase crystallized in the 'wehrlite' melt before its emplacement in the KEHLS magma chamber as sills or plugs. However, according to Tegner & Wilson (1993) and Tegner *et al.* (1993), the wehrlite suite can be divided into two groups, one as primary intrusives into the host layered gabbros, the other as secondary replacement bodies. The secondary group is abundant at Taco Point (see map, Fig. 2), where it occurs as complicated replacement structures around the primary (intrusive) wehrlite sills. Phlogopite is also present in the replacement wehrlites, but is undeformed and interstitial. In the present study, all samples of the wehrlite suite are of primary, intrusive nature.

Calculated liquid compositions of the sills and the wehrlite plug are presented in Fig. 12. The sills of the wehrlite suite (i.e. excluding the wehrlite plug sample 1610) display large variations in trace element contents. They do, however, form a coherent array. For example, whereas the Nd content ranges from 45 to 123 times chondrite, the Nd/Yb ratio only ranges from 3·9 to 4·3. Between Sr and Zr there is a marked positive correlation. It is also evident that the wehrlite sills have geochemical characteristics more in common with the cumulus and intercumulus melts from the gabbro suite (see below), than with the wehrlite plug sample 1610. Because of the primitive nature of sample 1610, featuring high *mg*-number in the mafic phases, high chromium in clinopyroxenes, high modal proportions of clinopyroxene and olivine, and low concentrations of incompatible elements, the melt composition of sample 1610 is regarded as representative of the melt parental to the wehrlite sills. Considering the genetic relationship between sample 1610 and the wehrlite sills, some process clearly modified the compositions of the sills.

Simple fractional crystallization of melt 1610 is unable to account for the discontinuous trends of the wehrlite suite (see Nd/Yb vs Nd and Sr vs Zr in Fig. 12). The field observations of soft sediment deformation around many of the wehrlite sills (Bernstein *et al.*, 1992), and the occurrence of replacive wehrlite bodies (Tegner & Wilson, 1993; Tegner *et al.*, 1993) point towards interaction between the intruding

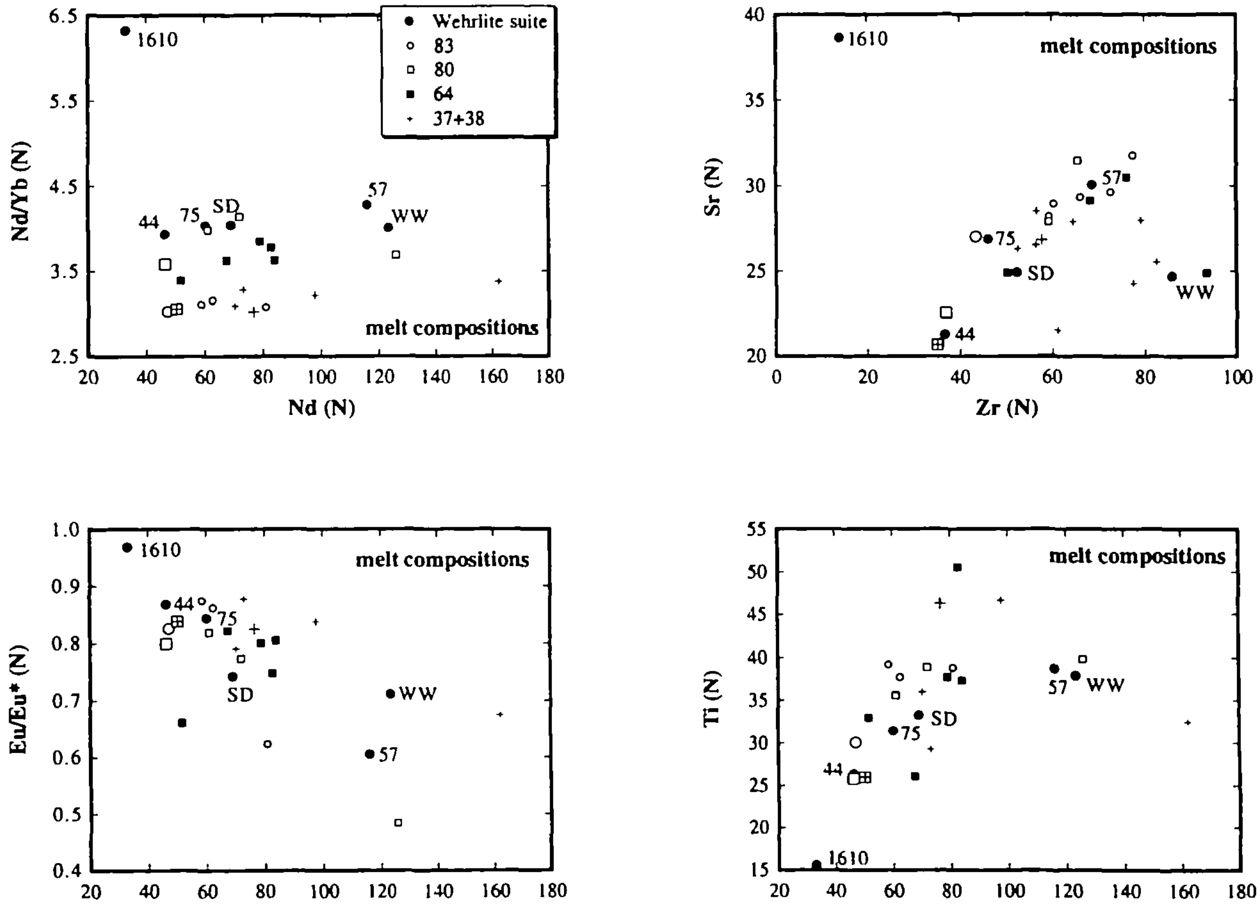

Fig. 12. Calculated liquid compositions of samples of the wehrlite suite, compared with equilibrium liquid compositions of all clinopyroxenes from the gabbro suite (excluding sample 61). For the gabbro suite, large symbols denote 'least evolved' compositions. 'Least evolved' compositions of wehrlite suite members are labelled with sample numbers.

wehrlite magma and the host layered gabbro, while interstitial liquid was still present in the gabbros. In Fig. 12 the compositions of all analysed clinopyroxenes from the gabbro suite (except sample 61, which is volumetrically unimportant) are included. The fractionated clinopyroxene analyses from the gabbro suite are taken as an approximation to the composition of intercumulus melt from the gabbro suite (small symbols). The wehrlite sills show patterns that are strikingly parallel to those defined by the cumulus and intercumulus melts from the gabbros, although displaced slightly towards the sample 1610 composition in the Nd/Yb vs Nd plot. The preliminary interpretation is that the wehrlite magma mixed or interacted with the gabbro mush during emplacement of the sills. The composition of the melt from which the first clinopyroxene crystallized appears to reflect the composition of the mixing component. For example, sill samples 44, 75 and perhaps SD mixed with relatively unfractionated melts from the gabbro suite, whereas the sills 57 and WW mixed with strongly evolved intercumulus melts. This observation corresponds well to the *mg*-number of the clinopyroxenes (Table 1), where samples 44 and 75 have highest *mg*-number, and samples SD, 57 and WW have lower *mg*-number.

Support for a mixing hypothesis for the chemical characteristics of the wehrlite sills comes from the composition of the deformed phlogopite crystals in the sills. From Fig. 13 it is noticed that there is little correlation between *mg*-number in mica and the average *mg*-number in coexisting clinopyroxene. In fact, the two sills, samples 57 and WW, that have some of the lowest *mg*-numbers in clinopyroxene and have the highest concentrations of incompatible elements among the wehrlite sills, have phlogopite crystals with some of the highest *mg*-numbers recorded, i.e. resembling the composition of the phlogopites from the wehrlite plug sample 1610. The tendency for phlogopites from the wehrlite sills to approach compositions of sample 1610 phlogopites is demonstrated in Fig. 14. To account for the range in phlogopite compositions, it is inferred that the phlogopite crystals, after or during emplacement of the sills, partly equilibrated with the infiltrating melt from the gabbro suite. Alternatively, low-temperature alteration may have resulted in loss of Mg, but the important point is that the wehrlite sill phlogopites are not in equilibrium with their coexisting clinopyroxenes, and originated as high *mg*-number phlogopites.

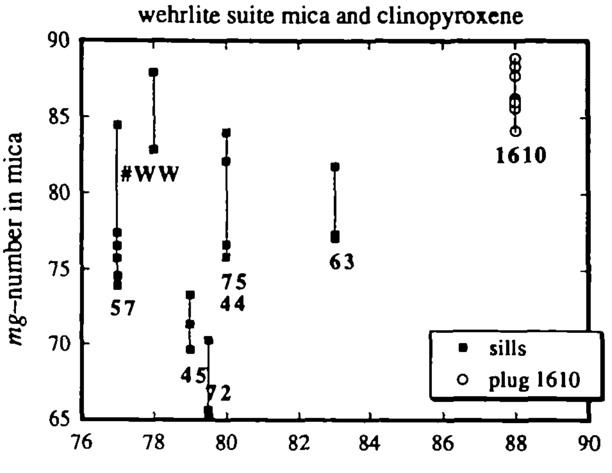

Fig. 13. Ranges in *mg*-number for phlogopite crystals from sills of the wehrlite suite, as a function of average *mg*-number of clinopyroxene from the same sample (solid symbols). [Note that clinopyroxenes from the samples 45, 63 and 72 have not been analysed by ion microprobe. The wehrlite plug sample 1610 (primitive end-member of the wehrlite suite) is represented by open symbols.

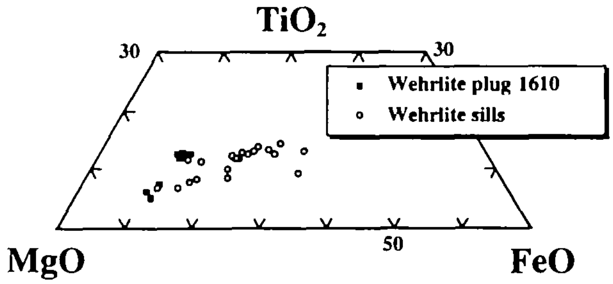

Fig. 14. Composition of phlogopite crystals from wehrlite sills (open circles) and wehrlite plug sample 1610 (solid squares). [Note the large variations in compositions of phlogopite from the sills, forming a continuous band from the primitive compositions of sample 1610 towards more Fe- and Ti-rich types.]

Additional information on possible mixing processes comes from the closely spaced sample set of layered gabbro and a wehrlite sill from the LLS. Sample 64 (gabbro suite) comes from a thick (> 150 m), uniform sequence of well-layered ol gabbros. Some 20 m above sample 64 is the 2 m thick wehrlite sill, sample 44. Clinopyroxene analyses of the two samples together with the least evolved analyses of wehrlite plug sample 1610 are presented in Fig. 15. The clinopyroxene compositions of sample 44 follow the trend of sample 64 closely, apart from the Nd/Yb ratios, which are higher for the most primitive sample 44 pyroxenes. The trace element pattern for the ol gabbro sample 64 is typical for the gabbro suite samples, reflecting early crystallization of mafic phases. It is considered unlikely that the chemistry of sample 64 was affected by the emplacement of the wehrlite sill, as that would require that large quantities of melt from the wehrlite sill migrated downward for tens of metres. Because of the uni-

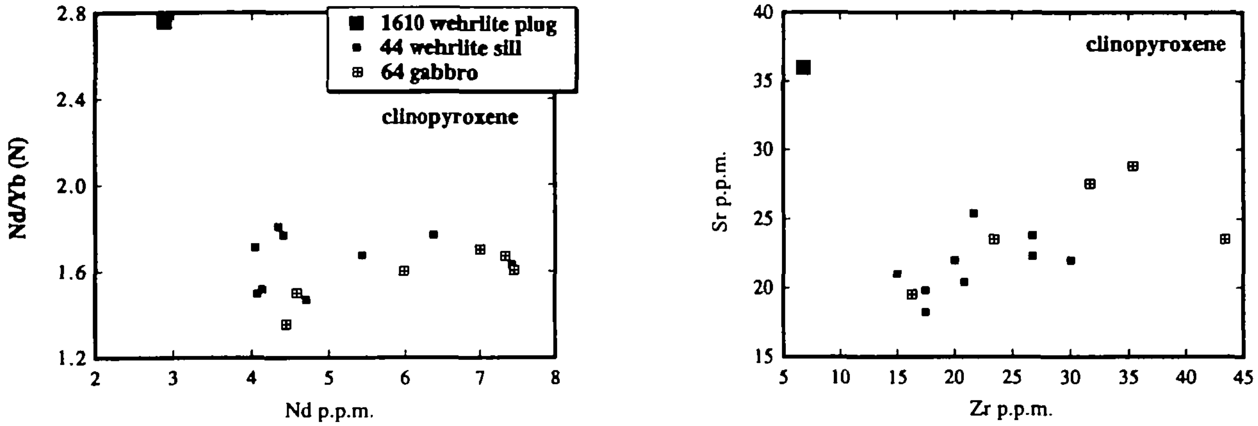

Fig. 15. All clinopyroxene analyses of the two neighbouring samples 64 (ol gabbro) and 44 (wehrlite sill). The 'least evolved' analyses of sample 1610 are given for comparison. The 1610 composition is believed to be parental to the 44 wehrlite sill. (Note the strong parallelism of the two trends.)

formity of the layered gabbro package in which sample 44 is found, sample 64 is representative of the gabbros hosting the wehrlite sill. The composition of the magma parental to the wehrlite sill (sample 44), may have approached that of the primitive gabbro during emplacement of the sill through mixing or reaction between incoming 'wehrlite' magma and the host gabbro mush. To account for the Nd/Yb ratios of the primitive sample 44 clinopyroxenes, about 1:1 mixing between sample 1610 and 64 melts is required. The high degree of mixing is supported by the very similar *mg*-numbers in clinopyroxenes from samples 44 and 64, and the higher modal proportions of plagioclase in the sill compared with the wehrlite plug sample 1610. Given that the variations in clinopyroxene composition occur within thin-section scale, it seems logical to preclude magma heterogeneities rising from the syn-emplacement mixing to be solely responsible for the trace-element patterns. Rather, the chemical patterns of the wehrlite sill clinopyroxenes appear to originate from infiltration of melts migrating from the gabbro mush. To acquire fractionation patterns practically identical to those of the host gabbros, mixing between liquid in the wehrlite sill and melts from the cumulus gabbro pile must have occurred during clinopyroxene crystallization, and this in turn requires a high flux of interstitial melt through the gabbro mush. The migration of melts through the wehrlite sill was allowed because the sill, by reaction–assimilation of maybe some 50% material from the host gabbro, had reached temperatures similar to the surroundings.

Similar processes are envisaged to be responsible for the chemical diversity of the wehrlite sills in general, and for their deviation from the chemistry of the wehrlite plug sample 1610. Migration of interstitial melt through a porous cumulus pile has long been known to be an important process in affecting the composition of cumulus rocks (e.g. Irvine, 1980; Tait *et al.*, 1984; Tait, 1985; Bédard *et al.*, 1988; Tegner & Wilson, 1993; Tegner & Robins, 1996). The recognition of extensive melt migration during the crystallization of the wehrlite sills confirms that they intruded while the KEHLS magma chamber was still hot enough for the gabbros to be above solidus. It also demonstrates that intercumulus melt migration must operate at least on the scale of several metres.

CONCLUSIONS

(1) Clinopyroxenes from the KEHLS mafic and ultramafic lithologies show large variations in trace-element concentrations and ratios, as revealed by ion microprobe analyses. The variations can largely be explained as a product of sequential fractional crystallization, with substantial crystallization of clinopyroxene (and possibly olivine) before plagioclase.

(2) The trace-element characteristics of the analysed clinopyroxenes confirm field observations that the KEHLS formed from at least two distinct magma types. One, termed the gabbro suite, from which the bulk of the intrusion crystallized, gave rise to anorthosites and olivine and oxide gabbros. The other, termed the wehrlite suite, was less abundant, comprising ultramafic and melanocratic sills and plugs intruding the solidifying gabbro suite.

(3) The composition of the liquids in equilibrium with clinopyroxene cores from the intermediate members of the gabbro suite can be related to the primitive end-member of the suite through RTF processes at elevated pressures (10–12 kbar). The more evolved members of the gabbro suite can be

related to the intermediate members through low-pressure ($\sim$2 kbar) RTF processes.

(4) Injection into the KEHLS of melts that evolved through RTF processes at elevated pressure before injection resulted in the formation of poikilitic anorthosites, owing to oversaturation in plagioclase. After precipitation of plagioclase, these melts evolved into crystallizing the 'normal' olivine and oxide gabbros.

(5) In terms of trace-elements, sills of the wehrlite suite show liquid compositions that are closely similar to estimated intercumulus liquids from the gabbro suite. Coupled with the field evidence, this suggests that interstitial liquids in large, slowly cooled layered intrusions migrate at a length scale of at least several metres.

(6) To accommodate the large quantities of fractionates inferred from the RTF model above, the deep-seated RTF-type magma chamber must be of considerable volume. If the pressure of fractionation refers to the transition between lower crust and upper mantle, then the crustal thickness at the time of emplacement (50 m.a.; Nevle *et al.*, 1993) of the KEHLS can be estimated to be $\sim$30 km. Given that the formation of oceanic crust at the proto-mid-Atlantic Ridge was well established by that time (Larsen, 1988), this implies that the transition between continental and oceanic crust is very abrupt around the Kangerlussuaq Fjord. With the evidence for the involvement of garnet in high-pressure ($>$15 kbar; equivalent to depth of 40–45 km) fractionation, for basalts of the Faeroe Lower Series (Bernstein, 1994, 1995) that were formed at 60–58 m.a. (Waagstein, 1988), it may be proposed that the thickness of the continental crust was reduced some 10–15 km during 8–10 m.y. of rifting.

ACKNOWLEDGEMENTS

We thank Nobu Shimizu for access to the ion microprobe facilities at WHOI, and for many fruitful discussions. Dennis K. Bird, Geoff Radford, Guy DellaValle, Karen Hanghøj and Andy Tuthill are thanked for assistance and company in the field, Bob Gannicott for logistical field support, and Christian Tegner for providing sample PCT 75. Assistance with the electron microprobe facilities at the Geological Institute by Jørn Rønsbo and John Fløng are much appreciated. Minik Rosing and Heidi Sjølin Thomsen are thanked for their support during the course of this work. Finally, we are grateful for critical comments on the manuscript by Christian Tegner and Ole Stecher, and for constructive reviews by S. A. Morse and K. G. Cox. S.B. acknowledges Danish Science Foundation Grant 11-8610, under which all the analytical work was carried out.

REFERENCES

Abbott, D. & Deer, W. A., 1972. Geological investigations in East Greenland. Part X. The gabbro cumulates of the Kap Edvard Holm Layered Series. *Meddelelser om Grønland* **190,** 1–41.

Barnes, S. J., 1986. The distribution of chromium among orthopyroxene, spinel and silicate liquid at atmospheric pressure. *Geochimica et Cosmochimica Acta* **50,** 1889–1909.

Bédard, J. H., Sparks, R. S. J., Renner, R., Cheadle, M. J. & Hallworth, M. A., 1988. Peridotite sills and metasomatic gabbros in the Eastern Layered Series of the Rhum complex. *Journal of the Geological Society of London* **145,** 207–224.

Bender, J. F., Hodges, F. N. & Barnes, A. E., 1978. Petrogenesis of basalts from the Project Famous Area: experimental study from 0 to 15 kbars. *Earth and Planetary Science Letters* **41,** 277–302.

Benn, K. & Laurent, R., 1987. Intrusive suite documented in the Troodos ophiolite plutonic complex, Cyprus. *Geology* **15,** 821–824.

Bernstein, S., 1994. High-pressure fractionation in rift-related basaltic magmatism: Faeroe plateau basalts. *Geology* **22,** 815–818.

Bernstein, S., 1995. Reply to Kerr, A. C. & Thompson, R. N., Comment on: High-pressure fractionation in rift-related basaltic magmatism: Faeroe plateau basalts. *Geology* **23,** 672.

Bernstein, S., Rosing, M. T., Brooks, C. K. & Bird, D. K., 1992. An ocean-ridge type magma chamber at a passive volcanic, continental margin: the Kap Edvard Holm layered gabbro complex, East Greenland. *Geological Magazine* **129,** 437–456.

Biggar, G. M., 1983. Crystallization of plagioclase, augite, and olivine in synthetic systems and in tholeiites. *Mineralogical Magazine* **47,** 161–176.

Bird, D. K., Manning, C. E. & Rose, N. M., 1988. Hydrothermal alteration of Tertiary layered gabbros, East Greenland. *American Journal of Science* **288,** 405–457.

Bird, D. K., Arnason, J. G., Brandriss, M. E., Nevle, R. J., Radford, G., Bernstein, S., Gannicott, R. G. & Kelemen, P. B., 1995. A gold-bearing horizon in the Kap Edvard Holm Complex, East Greenland. *Economic Geology* **90,** 1288–1300.

Bott, M. H. P., 1987. The continental margin of central East Greenland in relation to North Atlantic plate tectonic evolution. *Journal of the Geological Society of London* **144,** 561–568.

Brandeis, G., Jaupart, C. & Allègre, C. J., 1984. Nucleation, crystal growth and the thermal regime of cooling magmas. *Journal of Geophysical Research* **89,** 10161–10177.

Brooks, C. K. & Nielsen, T. F. D., 1982*a*. The Phanerozoic development of the Kangerdllugssuaq area, East Greenland. *Meddelelser om Grønland* **9,** 3–30.

Brooks, C. K. & Nielsen, T. F. D., 1982*b*. The E Greenland continental margin: a transition between oceanic and continental magmatism. *Journal of the Geological Society of London* **139,** 265–275.

Brooks, C. K., Nielsen, T. D. F. & Petersen, T. S., 1976. The Blosseville Coast basalts of East Greenland: their occurrence, composition, and temporal variations. *Contributions to Mineralogy and Petrology* **58,** 279–292.

Cox, K. G., 1988. Numerical modelling of a randomized RTF magma chamber: a comparison with continental flood basalt sequences. *Journal of Petrology* **29,** 681–697.

Deer, W. A. & Abbott, D., 1965. Clinopyroxenes of the gabbro cumulates of the Kap Edvard Holm complex, East Greenland. *Mineralogical Magazine* Tilley Volume, 177–193.

Drake, M. J. & Weill, D. F., 1975. Partition of Sr, Ba, Ca, Y, Eu^{2+}, Eu^{3+}, and other REE between plagioclase feldspar and magmatic liquid: an experimental study. *Geochimica et Cosmochimica Acta* **39**, 689–712.

Elsdon, R., 1969. The structure and intrusive mechanism of the Kap Edvard Holm layered gabbro complex, East Greenland. *Geological Magazine* **106**, 46–56.

Elsdon, R., 1971. Clinopyroxenes from the Upper Layered Series, Kap Edvard Holm, East Greenland. *Mineralogical Magazine* **38**, 49–57.

Fehlhaber, K. & Bird, D. K., 1991. Oxygen-isotope exchange and mineral alteration in gabbros of the Lower Layered Series, Kap Edvard Holm Complex, East Greenland. *Geology* **19**, 819–822.

Ford, C. E., 1981. Parental liquids of the Skaergaard intrusion cumulates. *Nature* **291**, 21–25.

Freer, R., 1981. Diffusion in silicate minerals and glasses: a data digest and guide to the literature. *Contributions to Mineralogy and Petrology* **76**, 440–454.

Fujii, T. & Bougault, H., 1983. Melting relations of a magnesian abyssal tholeiite and the origin of MORBs. *Earth and Planetary Science Letters* **62**, 283–295.

Fujimaki, H., Tatsumoto, M. & Aoki, K., 1984. Partition coefficients of Hf, Zr, and REE between phenocrysts and groundmasses. *Journal of Geophysical Research* **89**, B662–B672.

Furman, T., Frey, F. A. & Park, K.-H., 1991. Chemical constraints on the petrogenesis of mildly alkaline lavas from Vestmannaeyjar, Iceland: the Eldfeld (1973) and Surtsey (1963–1967) eruptions. *Contributions to Mineralogy and Petrology* **109**, 19–37.

Gallahan, W. E. & Nielsen, R. L., 1992. The partitioning of Sc, Y, and the rare earth elements between high-Ca pyroxene and natural mafic to intermediate lavas at 1 atmosphere. *Geochimica et Cosmochimica Acta* **56**, 2387–2404.

Grove, T. L. & Bryan, W. B., 1983. Fractionation of pyroxene-phyric MORB at low pressure: an experimental study. *Contributions to Mineralogy and Petrology* **84**, 293–309.

Grove, T. L., Kinzler, R. J. & Bryan, W. B., 1992. Fractionation of mid-ocean ridge basalt (MORB). In: Morgan, J. P., Blackman, D. K. & Sinton, J. M. (eds) *Mantle Flow and Melt Generation at Mid-ocean Ridges. Geophysical Monograph, American Geophysical Union* **71**, 281–310.

Hart, S. R. & Dunn, T., 1993. Experimental cpx/melt partitioning of 24 trace elements. *Contributions to Mineralogy and Petrology* **113**, 1–8.

Herzberg, C. T., 1978. Pyroxene geothermometry and geobarometry: experimental and thermodynamic evaluation of some subsolidus phase relations involving pyroxenes in the system $CaO–MgO–Al_2O_3–SiO_2$. *Geochimica et Cosmochimica Acta* **42**, 945–957.

Hogg, A. J. C., Fawcett, J. J., Gittins, J. & Gorton, M. P., 1988. Cyclical tholeiitic volcanism and associated magma chambers: eruptive mechanisms in E. Greenland. *Geological Society Special Publication* **39**, 197–200.

Hoover, J. D., 1978. Melting relations of a new chilled margin sample from the Skaergaard intrusion. *Carnegie Institution of Washington, Yearbook* **77**, 739–743.

Hoover, J. D., 1989. The chilled marginal gabbro and other contact rocks of the Skaergaard intrusion. *Journal of Petrology* **30**, 441–476.

Irvine, T. N., 1980. Magmatic infiltration metasomatism, double-diffusive fractional crystallization, and adcumulus growth in the Muskox intrusion and other layered intrusions. In: Hargraves, R. B. (ed.) *Physics of Magmatic Processes*. Princeton, NJ: Princeton University Press, pp. 325–383.

Irvine, T. N., 1987. Layering and related structures in the Duke Island and Skaergaard intrusions: similarities, differences and origins. In: Parsons, I. (ed.) *Origins of Igneous Layering*. Dordrecht: D. Reidel, pp. 196, 185–245.

Irving, A. J., 1978. A review of experimental studies of crystal/liquid trace element partitioning. *Geochimica et Cosmochimica Acta* **42**, 743–770.

Juteau, T., Ernewein, M., Reuber, I., Whitechurch, H. & Dahl, R., 1988. Duality of magmatism in the plutonic sequence of the Sumail Nappe, Oman. *Tectonophysics* **151**, 107–135.

Kelemen, P. B., Dick, H. J. B. & Quick, J. E., 1992. Formation of harzburgite by pervasive melt/rock reaction in the upper mantle. *Nature* **358**, 635–641.

Kirkpatrick, R. J., 1977. Nucleation and growth of plagioclase, Makaopuhi and Alae lava lakes, Kilauea Volcano, Hawaii. *Geological Society of America Bulletin* **88**, 78–84.

Kirkpatrick, R. J., 1983. Theory of nucleation in silicate melts. *American Mineralogist* **68**, 66–77.

Komor, S. C., Elthon, D. & Casey, J. F., 1987. Petrology of a leucogabbroic interval within basal layered gabbros at North Arm Mountain, Bay of Islands ophiolite. *Contributions to Mineralogy and Petrology* **95**, 278–300.

Larsen, H. C., 1988. A multiple and propagating rift model for the NE Atlantic. *Geological Society Special Publication* **39**, 278–300.

Larsen, L. M. & Watt, W. S., 1985. Episodic volcanism during break-up of the North Atlantic: evidence from the East Greenland plateau basalts. *Earth and Planetary Science Letters* **73**, 105–116.

Larsen, L. M., Watt, W. S. & Watt, M., 1989. Geology and petrology of the Lower Tertiary plateau basalts of the Scoresby Sund region, East Greenland. *Geological Survey of Greenland Bulletin* **157**, 1–164.

Lemarchand, F., Villemant, B. & Calas, G., 1987. Trace element distribution coefficients in alkaline series. *Geochimica et Cosmochimica Acta* **51**, 1071–1081.

McKay, G. A., 1989. Partitioning of rare earth elements between major silicate minerals and basaltic melts. In: Lipin, B. R. & McKay, G. A. (eds) *Geochemistry and Mineralogy of Rare Earth Elements. Mineralogical Society of America, Reviews in Mineralogy* **21**, 45–78.

McKay, G. A., Le, L. & Wagstaff, J., 1989. Redox conditions during the crystallization of unique achondrite LEW 86010. *Lunar and Planetary Science Conference* XX. Washington, DC: Mineralogical Society of America, pp. 677–678.

Morse, S. A. & Nolan, K. M., 1985. Kiglapait geochemistry VII: yttrium and the rare earth elements. *Geochimica et Cosmochimica Acta* **49**, 1621–1644.

Myers, J. S., 1980. Structure of the coastal dyke swarm and associated plutonic intrusions of East Greenland. *Earth and Planetary Science Letters* **46**, 407–418.

Myers, J. S., Gill, R. C. O., Rex, D. C. & Charnley, N. R., 1993. The Kap Gustav Holm plutonic centre, East Greenland. *Journal of the Geological Society of London* **150**, 259–276.

Nevle, R. J., Brandriss, M. E., Bird, D. K., McWilliams, M. O. & O'Neill, J. R., 1994. Tertiary plutons monitor climate change in East Greenland. *Geology* **22**, 775–778.

Nielsen, T. F. D., Soper, N. J., Brooks, C. K., Faller, A. M., Higgins, A. C. & Matthews, D. W., 1981. The pre-basaltic sediments and the Lower Basalts at Kangerdlugssuaq, East Greenland: their stratigraphy, lithology, palaeomagnetism and petrology. *Meddelelser om Grønland. Geoscience* **6**, 3–25.

O'Hara, M. J., 1977. Geochemical evolution during fractional crystallization of a periodically refilled magma chamber. *Nature* **266**, 503–507.

O'Hara, M. J. & Mathews, R. E., 1981. Geochemical evolution in an advancing, periodically replenished, periodically tapped, continuously fractionated magma chamber. *Journal of the Geological Society of London* **138**, 237–277.

Pallister, J. S. & Hopson, C. A., 1981. Samail ophiolite plutonic suite: field relations, phase variations, cryptic variation and layering, and a model of a spreading ridge magma chamber. *Journal of Geophysical Research* **86**, 2593–2644.

Paster, T. P., Schauwecker, D. S. & Haskin, L. A., 1974. The behaviour of some trace elements during solidification of the Skaergaard layered series. *Geochimica et Cosmochimica Acta* **38**, 1549–1577.

Pedersen, A. K., 1985. Reaction between picrite magma and continental crust: early Tertiary silicic basalts and magnesian andesites from Disko, West Greenland. *Bulletin Grønlands Geologiske Undersøgelse* **152**, 1–126.

Presnall, D. C., Dixon, S. A., Dixon, J. R., O'Donnell, T. H., Brenner, N. L., Schrock, R. L. & Dycus, D. W., 1978. Liquidus phase relations on the join diopside–forsterite–anorthosite from 1 atm to 20 kbar: their bearing on the generation and crystallization of basaltic magmas. *Contributions to Mineralogy and Petrology* **66**, 203–220.

Roeder, P. L. & Emslie, R. F., 1970. Olivine–liquid equilibrium. *Contributions to Mineralogy and Petrology* **29**, 275–289.

Scowen, P. A. H., Roeder, P. L. & Helz, R. T., 1991. Reequilibration of chromite within Kilauea Iki lava lake, Hawaii. *Contributions to Mineralogy and Petrology* **107**, 8–20.

Shimizu, N., 1981. Trace element incorporation into growing augite phenocryst. *Nature* **289**, 575–577.

Shimizu, N. & Le Roex, A. P., 1986. The chemical zoning of augite phenocrysts in alkaline basalts from Gough Island, South Atlantic. *Journal of Volcanology and Geothermal Research* **29**, 159–188.

Shimizu, N., Semet, M. P. & Allègre, C. J., 1978. Geochemical applications of quantitative ion-microprobe analysis. *Geochimica et Cosmochimica Acta* **42**, 1321–1334.

Soper, N. J., Downie, C., Higgins, A. C. & Costa, L. I., 1976. Biostratigraphic ages of Tertiary basalts on the East Greenland continental margin and their relationship to plate separation in the Northeast Atlantic. *Earth and Planetary Science Letters* **32**, 149–157.

Sun, S.-S. & McDonough, W. F., 1989. Chemical and isotopic systematics of oceanic basalts: implications for mantle composition and processes. *Geological Society Special Publication* **42**, 313–345.

Sun, S.-S., Nesbitt, R. W. & Sharaskin, A. Y., 1979. Geochemical characteristics of mid-ocean ridge basalts. *Earth and Planetary Science Letters* **44**, 119–138.

Tait, S. R., 1985. Fluid dynamic and geochemical evolution of cyclic unit 10, Rhum, Eastern Layered Series. *Geological Magazine* **122**, 469–484.

Tait, S. R., Huppert, H. E. & Sparks, R. S. J., 1984. The role of compositional convection in the formation of adcumulate rocks. *Lithos* **17**, 139–146.

Tegner, C. & Robins, B., 1996. Picrite sills and crystal–melt reactions in the Honningsvåg Intrusive Suite, northern Norway. *Mineralogical Magazine* **60**, 53–66.

Tegner, C. & Wilson, J. R., 1993. A late ultramafic suite in the Kap Edvard Holm layered gabbro complex, East Greenland. *Geological Magazine* **130**, 431–442.

Tegner, C. & Wilson, J. R., 1995. Textures in a poikilitic olivine gabbro cumulate: evidence for supercooling. *Mineralogy and Petrology* **54**, 161–173.

Tegner, C., Wilson, J. R. & Brooks, C. K., 1993. Intraplutonic quench zones in the Kap Edvard Holm layered gabbro complex, East Greenland. *Journal of Petrology* **34**, 681–710.

Thy, P., 1991. High and low pressure phase equilibria of a mildly alkalic lava from the 1965 Surtsey eruption: experimental results. *Lithos* **26**, 223–243.

Vannucci, R., Rampone, E., Piccardo, G. B., Ottolini, L. & Bottazzi, P., 1993. Ophiolitic magmatism in the Ligurian Tethys: an ion microprobe study of basaltic clinopyroxenes. *Contributions to Mineralogy and Petrology* **115**, 123–137.

Villemant, B., Jaffrezic, H., Joron, J.-L. & Treuil, M., 1981. Distribution coefficients of major and trace elements; fractional crystallization in the alkali basalt series of Chaîne des Puys (Massif Central, France). *Geochimica et Cosmochimica Acta* **45**, 1997–2016.

Waagstein, R., 1988. Structure, composition and age of the Faeroe basalt plateau. *Geological Society Special Publication* **39**, 225–238.

Wager, L. R., 1934. Geological investigations in East Greenland. Part 1. General geology from Angmagssalik to Kap Dalton. *Meddelelser om Grønland* **105**, 1–46.

Wager, L. R., 1947. Geological investigations in East Greenland, Part IV: the stratigraphy and tectonics of Knud Rasmussens Land and the Kangerdlugssuaq region. *Meddelelser om Grønland* **134**, 1–64.

Wager, L. R., 1960. The major element variation of the layered series of the Skaergaard intrusion and a re-estimation of the average composition of the hidden layered series and of the successive residual magmas. *Journal of Petrology* **1**, 364–398.

Wager, L. R. & Brown, G. M., 1968. *Layered Igneous Rocks*. London: Oliver and Boyd.

Watson, E. B. & Baker, D. R., 1992. Chemical diffusion in magmas: an overview of experimental results and geochemical applications. In: Perchuk, L. L. & Kushiro, I. (eds) *Physical Chemistry of Magmas*. Heidelberg: Springer-Verlag, pp. 120–151.

Wilson, M., 1989. *Igneous Petrogenesis*. London: Chapman and Hall.

Wood, B. J., 1976. Mixing properties of tschermakitic clinopyroxenes. *American Mineralogist* **61**, 599–602.

RECEIVED JULY 15, 1995
REVISED TYPESCRIPT ACCEPTED JANUARY 1, 1996